Calhoun: The NPS Institutional Archive

DSpace Repository

Theses and Dissertations | 1. Thesis and Dissertation Collection, all items

2009-03

Characterization of episodic rip current pulsations in the inner shelf during RCEX 2007

O'Neill, Andrea C.

Monterey, California. Naval Postgraduate School

https://hdl.handle.net/10945/4799

Downloaded from NPS Archive: Calhoun

http://www.nps.edu/library

Calhoun is the Naval Postgraduate School's public access digital repository for research materials and institutional publications created by the NPS community. Calhoun is named for Professor of Mathematics Guy K. Calhoun, NPS's first appointed -- and published -- scholarly author.

Dudley Knox Library / Naval Postgraduate School
411 Dyer Road / 1 University Circle
Monterey, California USA 93943

NAVAL POSTGRADUATE SCHOOL

MONTEREY, CALIFORNIA

THESIS

CHARACTERIZATION OF EPISODIC RIP CURRENT PULSATIONS IN THE INNER SHELF DURING RCEX 2007

by

Andrea C. O'Neill

March 2009

Thesis Advisor:	Jamie MacMahan
Second Reader	Edward B. Thornton

Approved for public release; distribution is unlimited.

THIS PAGE INTENTIONALLY LEFT BLANK

REPORT DOCUMENTATION PAGE		Form Approved OMB No. 0704-0188

Public reporting burden for this collection of information is estimated to average 1 hour per response, including the time for reviewing instruction, searching existing data sources, gathering and maintaining the data needed, and completing and reviewing the collection of information. Send comments regarding this burden estimate or any other aspect of this collection of information, including suggestions for reducing this burden, to Washington headquarters Services, Directorate for Information Operations and Reports, 1215 Jefferson Davis Highway, Suite 1204, Arlington, VA 22202-4302, and to the Office of Management and Budget, Paperwork Reduction Project (0704-0188) Washington DC 20503.

1. AGENCY USE ONLY *(Leave blank)*	2. REPORT DATE	3. REPORT TYPE AND DATES COVERED
	March 2009	Master's Thesis

4. TITLE AND SUBTITLE Characterization of Episodic Rip Current Pulsations in the Inner Shelf during RCEX 2007	5. FUNDING NUMBERS
6. AUTHOR(S) Andrea O'Neill	
7. PERFORMING ORGANIZATION NAME(S) AND ADDRESS(ES) Naval Postgraduate School Monterey, CA 93943-5000	8. PERFORMING ORGANIZATION REPORT NUMBER
9. SPONSORING /MONITORING AGENCY NAME(S) AND ADDRESS(ES) N/A	10. SPONSORING/MONITORING AGENCY REPORT NUMBER

11. SUPPLEMENTARY NOTES The views expressed in this thesis are those of the author and do not reflect the official policy or position of the Department of Defense or the U.S. Government.

12a. DISTRIBUTION / AVAILABILITY STATEMENT	12b. DISTRIBUTION CODE
Approved for public release; distribution is unlimited.	

13. ABSTRACT (maximum 200 words)

As the Navy thrusts operations into global "brown water" environments, a more complete understanding of the phenomena ships and swimmers will encounter in nearshore regions is necessary. Rip currents remain infamous and important characteristics of the nearshore environment. These events not only impinge upon swimmers' safety, but may play a key role transferring water, containing nutrients, biologics, and even shore-/ship-borne pollution, between the surf zone and open ocean environments. Vertical and temporal behavior of rip currents outside of the surf zone is poorly understood due to a paucity of comprehensive observations. Observations of two upward-looking Acoustic Doppler Current Profilers (ADCP) deployed in 3 m and 5 m water depth within a rip current (nominally 1.0 and 1.2 surf zone widths from the shoreline respectively) were obtained during April-May 2008 as part of the Rip Current EXperiment (RCEX) at Sand City, Monterey Bay, CA. The ADCPs sampled continuously at 1 Hz. Energetic seaward-directed episodic pulses associated with the rip current obtained velocities up to 0.5 m/s with a frequency of occurrence varying from 1-15 times a day depending upon coincident wave and tidal conditions. Vertical variations of the episodic rip current pulsations ranged depth-uniform to surface-dominated. Cross-rotary analysis and complex correlation, performed in the vertical to describe rotational behavior and temporal lags, show rip currents in the inner shelf exhibit more rotation, up to 20 degrees in both CW and CCW directions, than in the surf zone. High coherence is limited to near-surface levels in the inner shelf, versus more depth-uniform values in the surf zone. Mean vertical profiles show these phenomena exhibit significant shear and structure.

14. SUBJECT TERMS Rip currents, rip current structure, episodic rip current pulsations, inner shelf, RCEX 2007, surf zone volume exchange, Sand City, nearshore circulation	15. NUMBER OF PAGES 63
	16. PRICE CODE

17. SECURITY CLASSIFICATION OF REPORT	18. SECURITY CLASSIFICATION OF THIS PAGE	19. SECURITY CLASSIFICATION OF ABSTRACT	20. LIMITATION OF ABSTRACT
Unclassified	Unclassified	Unclassified	UU

NSN 7540-01-280-5500

Standard Form 298 (Rev. 8-98)
Prescribed by ANSI Std. Z39.18

THIS PAGE INTENTIONALLY LEFT BLANK

Approved for public release; distribution is unlimited.

CHARACTERIZATION OF EPISODIC RIP CURRENT PULSATIONS IN THE INNER SHELF DURING RCEX 2007

Andrea C. O'Neill
Lieutenant, United States Navy
B.S., University of Washington, 2001

Submitted in partial fulfillment of the
requirements for the degree of

MASTER OF SCIENCE IN METEOROLOGY AND PHYSICAL OCEANOGRAPHY

from the

NAVAL POSTGRADUATE SCHOOL
March 2009

Author: Andrea C. O'Neill

Approved by: Jamie MacMahan
Thesis Advisor

Edward B. Thornton
Second Reader

Jeffrey D. Paduan
Chairman, Department of Oceanography

THIS PAGE INTENTIONALLY LEFT BLANK

ABSTRACT

As the Navy thrusts operations into global “brown water” environments, a more complete understanding of the phenomena ships and swimmers will encounter in nearshore regions is necessary. Rip currents remain infamous and important characteristics of the nearshore environment. These events not only impinge upon swimmers’ safety, but may play a key role transferring water, containing nutrients, biologics, and even shore-/ship-borne pollution, between the surf zone and open ocean environments. Vertical and temporal behavior of rip currents outside of the surf zone is poorly understood due to a paucity of comprehensive observations. Observations of two upward-looking Acoustic Doppler Current Profilers (ADCP) deployed in 3 m and 5 m water depth within a rip current (nominally 1.0 and 1.2 surf zone widths from the shoreline respectively) were obtained during April-May 2008 as part of the Rip Current EXperiment (RCEX) at Sand City, Monterey Bay, CA. The ADCPs sampled continuously at 1 Hz. Energetic seaward-directed episodic pulses associated with the rip current obtained velocities up to 0.5 m/s with a frequency of occurrence varying from 1-15 times a day depending upon coincident wave and tidal conditions. Vertical variations of the episodic rip current pulsations ranged depth-uniform to surface-dominated. Cross-rotary analysis and complex correlation, performed in the vertical to describe rotational behavior and temporal lags, show rip currents in the inner shelf exhibit more rotation, up to 20 degrees in both CW and CCW directions, than in the surf zone. High coherence is limited to near-surface levels in the inner shelf, versus more depth-uniform values in the surf zone. Mean vertical profiles show these phenomena exhibit significant shear and structure.

THIS PAGE INTENTIONALLY LEFT BLANK

TABLE OF CONTENTS

I. INTRODUCTION 1

II. METHODOLOGY 7
- A. RCEX DATA 7
- B. DEPTH-RELATIVE NORMALIZATION 7
- C. SPECTRAL ANALYSIS 8
- D. CROSS-ROTARY ANALYSIS 10
- E. COMPLEX CORRELATION 12
- F. GROUP-AVERAGING 14
- G. STOKES DRIFT CHECK 15
- H. WAVELET ANALYSIS 17

III. RESULTS 19
- A. SPECTRA/RMS 19
- B. CROSS-ROTARY ANALYSIS 20
- C. COMPLEX CORRELATION 23
- D. GROUP-AVERAGING 25
- E. STOKES DRIFT 26

IV. DISCUSSION 27

V. CONCLUSIONS AND RECOMMENDATIONS 31

APPENDIX A. CROSS-ROTARY ANALYSIS 35

APPENDIX B. COMPLEX CORRELATION 37

APPENDIX C. WAVELET ANALYSIS 39

LIST OF REFERENCES 45

INITIAL DISTRIBUTION LIST 49

THIS PAGE INTENTIONALLY LEFT BLANK

LIST OF FIGURES

Figure 1. RCEX bathymetry and instrument layout for the cross-shore, bottom-mounted array. Distances alongshore and cross-shore are labeled in meters; ADCPs are numerically labeled in an offshore direction. ADCPs recorded velocity data continuously (1 Hz sampling rate) for 19 days in April-Mary 2007 in Sand City, CA. The array was centered in a rip current channel stretching out to 150 m from the shore. Nortek ADCP 4 (2 MHz) and RDI ADCP 6 (1.2 MHz) are used in this study. ADCP 4 and ADCP 6 were deployed in water depths of 3 m and 5 m respectively. The red line depicts the average extent of the surfzone; actual extent depended on daily wave and tide conditions 4

Figure 2. Conditions of wave height, wave period, and tidal elevation at ADCP 4 during RCEX. High-energy wave conditions (>1.1m) occurred on days 123-126, 134, and 140. Blank periods are due to instrumentation problems. 5

Figure 3. Near-surface (blue) and near-bottom (red) very low frequency (VLF, <.004 Hz) U for days 123 and 128 at ADCP 6 and ADCP 4. Energetic pulses (offshore-directed velocities > 0.1 m/s) occurred 1-15 times a day at ADCP 6. Day 123 (top) illustrates high-energy wave conditions (> 1.1m); day 128 illustrates low-energy wave conditions (< 1.0m). 6

Figure 4. Hourly mean U (top), 3-hour VLF root mean square (rms) U (middle), and VLF V_{rms} (bottom) for ADCP 6 (left) and ADCP 4 (right). The red line in ADCP 4 mean U denotes when the instrument location is within the surf zone ($H_{rms}/h > 0.3$). 9

Figure 5. VLF band-averaged cross-spectral coherence and phase for ADCP 6 and ADCP 4. Values are computed between near-surface and near-bottom levels for 3-hour intervals. Reference levels (1.0 coherence) are near-surface for ADCP 6 and near-bottom for ADCP 4. Phase values are plotted for coherence values above 95% significance level. 10

Figure 6. VLF band-averaged XROT inner (co-rotating series, top two rows) and outer (counter-rotating, bottom two rows) coherence and phase for positive (CCW) frequencies. Phase values are plotted for coherence levels above 95% significance level. 11

Figure 7. Same as Figure 6 for negative (CW) frequencies. 12

Figure 8. Bulk complex correlation values for ADCP 6 (left) and ADCP 4 (right), showing mid-column (circle) and full-column (diamond) relationships. Correlation (top row) is shown versus H_{rms} (root mean square wave height), while the phase (middle row) and shear (U difference, bottom row) of each pulse is shown versus time lead/lag (τ). 13

Figure 9. Group-averaged U profiles (left) and standard deviations (right) for ADCP 6. Profiles are determined from VLF U. Offshore velocities are negative. 14
Figure 10. Same as Figure 9 for ADCP 4. Profiles are determined from bandpass-filtered (0.0005-0.004 Hz) U. 15
Figure 11. Scatterplot of one-hour mean values of calculated shoreward transport (from U) versus theoretical shoreward transport (Stokes drift) estimates at ADCP 4. Solid circles denote instances where wave and height conditions placed ADCP 4 in the surf zone. The blue dashed line denotes a one-to-one relationship. Regression relationship for when ADCP 4 is not in surf zone (open circles) is 0.78. 17
Figure 12. One-hour mean theoretical shoreward transport (Stokes drift) estimates (dashed blue line), calculated shoreward transport (solid blue line), calculated offshore transport (red line), and net transport values (green line) for RCEX. Net transport values are determined from theoretical shoreward and calculated offshore values. Offshore values are negative. 27
Figure 13. Conceptual drawing of surf zone inputs and outputs for purposes of calculating flushing time and volume flux. The surf zone has volume inputs from Stokes drift and outputs in rip pulses. 28
Figure 14. XROT wavelet analysis for synthetic pulse. Color indicates the phase angle (in degrees) between the corotating components of both series. Phase is only plotted where the co-rotating coherence is above 0.7. Shaded regions outside the COI show where edge effects are important. Period (in days) is plotted along the y axis while time (in Julian day) is plotted along the x axis. Red arrows indicate the time of the maximum pulse velocity. 43

ACKNOWLEDGMENTS

I would like to thank my Thesis advisor, Professor Jamie MacMahan, for all his guidance. Additionally, thanks to Professor Edward Thornton and Ad Reniers, who reviewed my work in Thesis and poster form for the AGU Conference; your input was invaluable. To Mike Cook, thank you for all your instruction, patience, and assistance.

No matter how wonderful the instruction and mentorship of NPS professors, though, friends get you through the tough and trying times, so thank you to all my friends who helped make life bearable during these fun months. John Hendrickson, always my companion in MATLAB misery, thank you and good luck. As well, the same goes out to the rest of my class-mates experiencing their own thesis-related stress: Mike, Dimtrios, Brian, Rick, and Jackie. I think we had one of the best sections. Last but not least, Patrick rocks.

To my husband, Nick, your support and devotion give me strength. Thank you.

THIS PAGE INTENTIONALLY LEFT BLANK

I. INTRODUCTION

Rip currents are infamous, yet important, features in the nearshore environment. For many seaside visitors, rip currents conjure images of swimmers being swept out to sea by powerful and unyielding currents. While rip currents can pose a risk to the unwary swimmer, they also are a key feature in the circulation of the nearshore region. Rip currents play a central role in the water exchange between the surf zone, the area shoreward of breaking waves, and the open ocean (Haas and Svendsen, 2002; MacMahan et al., 2006; Shepard et al., 1941; and Smith and Largier, 1995). These powerful currents can eject biologic material, organisms, sediment, pollution, as well as swimmers (Grant, et al, 2005; MacMahan et al., 2009; and Shepard et al., 1941), from the well-mixed surf zone to the inner shelf, a shallow region just beyond the breakers where surface and bottom boundary conditions interact, and farther out to sea.

Rip currents, ubiquitous to many morphologically different beaches around the world, are strong seaward, non-continuous currents flowing normal to the shoreline. Violent speeds and mixing create the turbid waters just beyond the surf zone, full of suspended material and bubbles, which can often visually identify a rip current. The rip head, found outside the surf zone, is the seaward extent of the rip current, originated by alongshore variations in momentum flux (Haas and Svendsen, 2002; MacMahan et al., 2006).

While coastal research has continued to improve understanding of rip currents within the surf zone environment, rip currents beyond the surf zone remain poorly understood, mainly due to a lack in comprehensive observations. Smith and Largier (1995) observed that rip currents occur as episodic jets and detach from the surf zone when flowing offshore. As their observations only included a few vertical profiles of conductivity, temperature, and turbidity outside the rip current, little else could be determined of the vertical structure. Laboratory experiments have attempted to model the dynamics in this region and have given

some insight into the rip current structure; Haas and Svendsen (2002) have shown that rip currents beyond the surf zone may exhibit rotation in the vertical structure and predominantly flow near the surface. Field data of rip currents remain sparse, due not only to the energetic nature of the nearshore environment, but also the nature of rip currents. Rip currents do not stay confined to one path through the rip channel, but meander in the along-shore direction within the channel (Haller and Dalrymple, 2001; MacMahan et al., 2005). Any improvement of understanding into the nature of rip currents in the surf zone boundary to inner shelf would advance understanding of the cross-shelf exchange between these regions.

An improved understanding of the volume exchange between surf zone and inner shelf regions would benefit coastal communities and all those operating in the nearshore region, such as the Navy. In an increasingly environmentally aware culture, conscientious handling of operational discharge and by-products is a priority in order to prevent spills and spreading of contaminants into biologically sensitive environments. For coastal communities, non-point source pollution from runoff poses the major concern. The ocean regions neighboring large populations act as the “final repository of human waste” (Grant et al., 2005), increasing the concentrations of fecal and other illness-causing bacteria in the nearshore. This narrow nearshore region is also where the vast majority of recreational and work-related activity takes place (Grant et al., 2005), increasing human health hazards. Knowledge of the manner and pace in which any shore-borne or ship-borne contaminant transfers from the surf zone into the inner shelf and open ocean is crucial for taking proper care and action to avoid human health and ecosystem disasters.

Rip currents flush not only anthropogenic material from the surf zone, but biologic matter as well. Some species of dinoflagellates, better known to mariners and Sailors as the sparkle in fluorescent waters (Rohr et al., 2002; Stokes et al., 2004), thrive in the well-mixed surroundings of the surf zone. Strong rip currents could flush the surf zone and increase concentrations of

fluorescence in the inner shelf, possibly giving away the wake of a small boat or swimmer/diver (Rohr et al., 2002). Naval swimmers also have to contend with decreased visibility from the biologic particulate and sediment suspended in the current. In addition to the physical obstacle posed by a rip current, knowledge of such optical complications is essential to any plan for a “brown water” (close to shore) or Naval Special Warfare operation along a beach.

In 2007, Rip Current EXperiment (RCEX) was conducted in Sand City, CA, to make detailed observations in the surf zone and inner shelf environments in order to capture the characteristics of flow and circulation in the nearshore region. Morphology at Sand City is comprised of shore-connected shoals with incised rip channels. The rip currents are defined to be open coast rip currents, as there are no offshore structures to impede or influence the rip system (MacMahan et al., 2005). The experiment employed a cross-shore array of stationary Acoustic Doppler Current Profilers (ADCP) (Figure 1) and pressure sensors in addition to 30 GPS-tracking drifters. Drifter data showed clear rip current cells persistent in the experiment area. During the course of the experiment, MacMahan noticed that drifters were occasionally pushed offshore, beyond the extent of rip current cells and into the inner-shelf. Inspection of ADCP data 50 meters beyond the surf zone during those times showed episodic offshore-directed pulses up to 0.5 m/s in magnitude. These episodic pulses are observed in the ADCP data throughout the experiment time period for a variety of wave and tidal conditions (Figure 2).

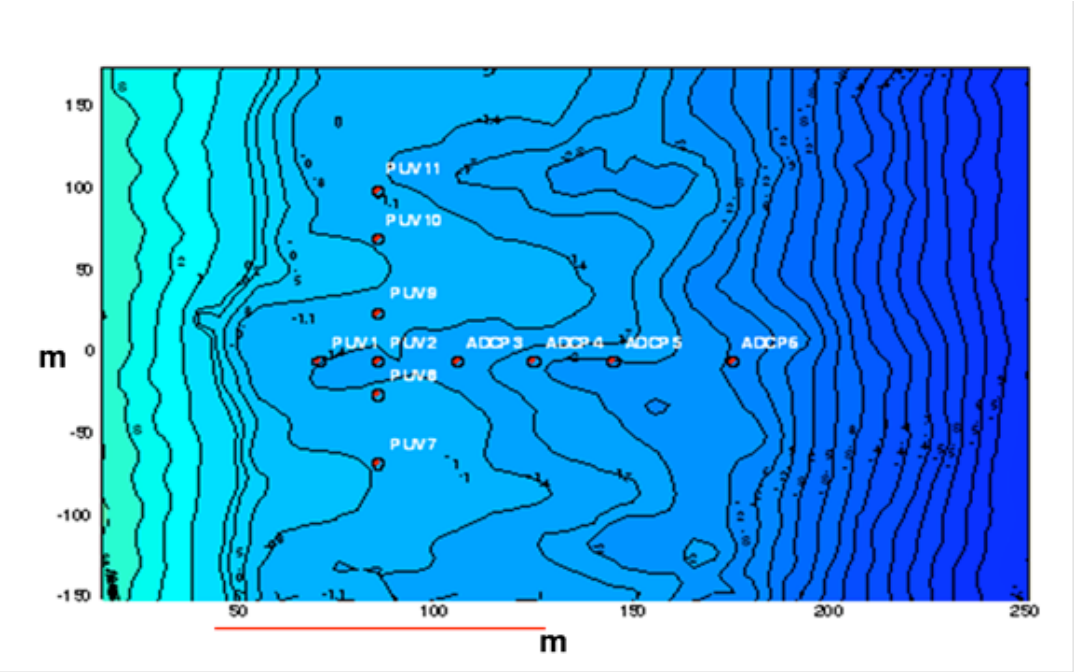

Figure 1. RCEX bathymetry and instrument layout for the cross-shore, bottom-mounted array. Distances alongshore and cross-shore are labeled in meters; ADCPs are numerically labeled in an offshore direction. ADCPs recorded velocity data continuously (1 Hz sampling rate) for 19 days in April-Mary 2007 in Sand City, CA. The array was centered in a rip current channel stretching out to 150 m from the shore. Nortek ADCP 4 (2 MHz) and RDI ADCP 6 (1.2 MHz) are used in this study. ADCP 4 and ADCP 6 were deployed in water depths of 3 m and 5 m respectively. The red line depicts the average extent of the surfzone; actual extent depended on daily wave and tide conditions

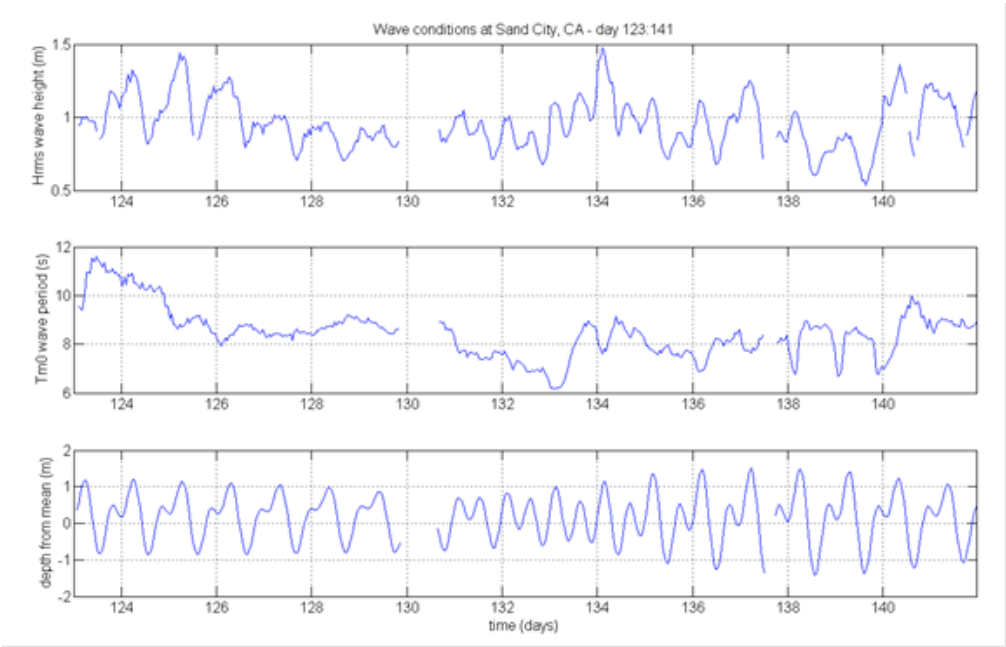

Figure 2. Conditions of wave height, wave period, and tidal elevation at ADCP 4 during RCEX. High-energy wave conditions (>1.1m) occurred on days 123-126, 134, and 140. Blank periods are due to instrumentation problems.

In the horizontal, it is assumed these pulses spatially resemble the rip currents observed by Smith and Largier (1995); however, energetic pulses (velocity > 0.1 m/s) vary in time, intensity and vertical structure, occurring 1 to 15 times a day (frequency < 0.004 Hz) 50 m beyond the surf zone (Figure 3). Two broad groups encompass the observed pulse variation: 1) those fairly uniform in the vertical structure, having similar current magnitudes near the surface and near the bottom, and 2) surface-dominated currents where high velocities are predominantly observed near the surface.

The effort of this study was to quantitatively analyze and characterize these pulsations in and out of the surf zone, specifically to gain insight into the temporal and rotational characteristics of the episodic phenomenon. To localize this study and focus on the differences between surf zone and inner shelf environments, data from two ADCPs were used: ADCP 4 located at the offshore edge of the surf zone, and ADCP 6 located 50 m beyond the surf zone in the inner shelf (Figure 1).

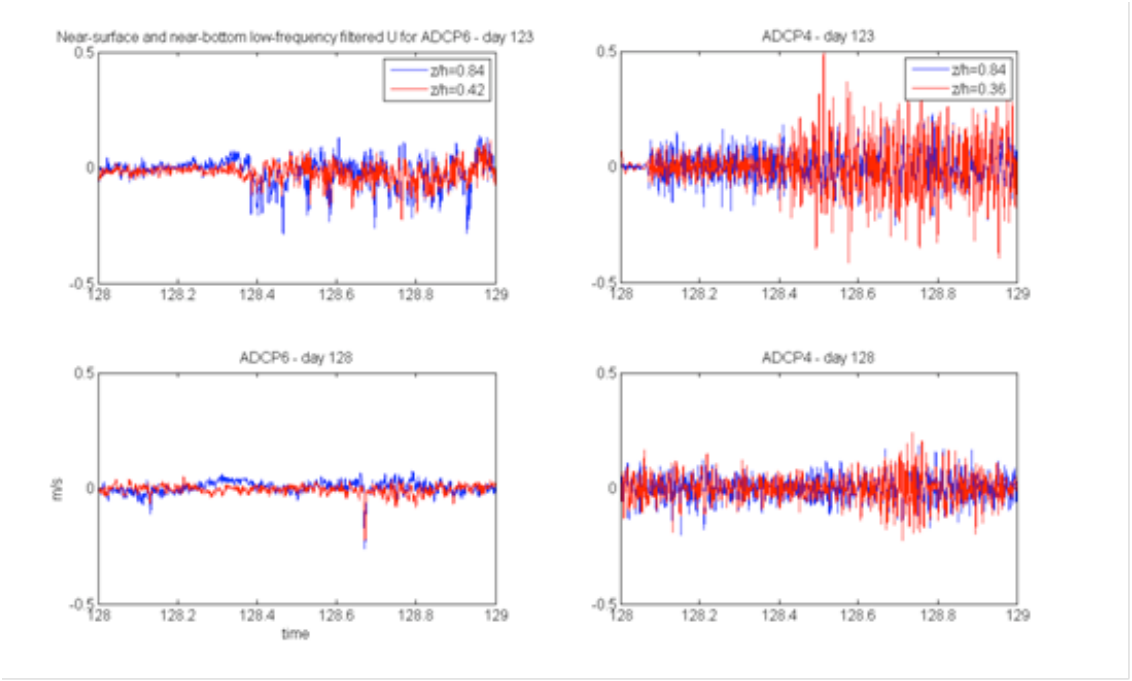

Figure 3. Near-surface (blue) and near-bottom (red) very low frequency (VLF, <.004 Hz) U for days 123 and 128 at ADCP 6 and ADCP 4. Energetic pulses (offshore-directed velocities > 0.1 m/s) occurred 1-15 times a day at ADCP 6. Day 123 (top) illustrates high-energy wave conditions (> 1.1m); day 128 illustrates low-energy wave conditions (< 1.0m).

II. METHODOLOGY

A. RCEX DATA

ADCPs emit an acoustic pulse, which scatters off particles (such as sand, biologic matter, and bubbles) suspended within the water column ("Acoustic Doppler Current Profiler," 1989). Using the scattered signal returns and the Doppler shift principle, the ADCP can calculate the velocity of the water at various elevations within the water column, making it an invaluable tool for investigating vertical current structure. RCEX employed three RDI ADCPs (1.2 MHz), one Nortek ADCP (2 MHz), and two pressure sensors as part of a cross-shore, bottom-mounted sensor array. The array was centered in a rip current channel at Sand City, CA, stretching out to 150 m from the shore (Figure 1). ADCP 6 (RDI), was located approximately 50 m beyond the surf zone in the inner shelf, and ADCP 4 (Nortek) was on the border between these regions. ADCP 4 and 6 were deployed in water depths relative to mean sea level (MSL) of 3 m and 5 m respectively.

ADCPs continuously sampled velocity in the water column at 1 Hz, using a bin depth of 0.5 m, for 19 days during April-May of 2007. Sample times were documented in Julian Day. ADCP data were corrected for surface elevation using data from collocated pressure sensors. Sea-surface elevations were obtained using linear wave theory transformations. The data were then rotated to local cross- (U) and along-shore (V) velocity components, respectively shore-normal and shore-parallel.

B. DEPTH-RELATIVE NORMALIZATION

The U and V velocity data were then normalized in a depth-relative framework. Instead of using velocities for a corresponding depth or ADCP bin, velocities were interpolated to a ratio scale giving the height in the water column (z) versus the depth of water (h) at the location. The scale was ordered 0 to 1.5,

with 0 at the bottom and 1.5 at the top of a high wave crest. To account for tidal action and low-frequency infragravity waves on the water depth of the location, h was calculated by including the low-frequency sea-surface oscillations (f < 0.04 Hz). Accounting for tidal variability, this technique allowed for direct comparison of results between instruments and between different times within the tidal cycle using the same instrument, as the data at the locations would be in the same relative position in the water column. Two depth-relative levels in the water column were primarily used in this study to examine rotational effects in the pulses: a near-surface and a near-bottom "depth". The near-surface level at 0.84 corresponded to the maximum offshore-directed velocity while remaining below the influence of surface wave action over the entire exercise period. The near-bottom level was taken to be 0.42 for ADCP 6, which is the lowest sampled level in the water column due to the bottom-mounting height and RDI ADCP blanking distance. For consistency, a near-bottom depth of 0.36 was used for ADCP 4.

C. SPECTRAL ANALYSIS

Single spectra and cross-spectra analysis were performed on three-hour intervals of U and V to examine columnar relationships in velocity. An interval of three hours was used to capture the signatures of the pulses while minimizing the bias from changes in tidal elevation. This interval was determined to be the minimum time required to obtain a statistically significant number of pulses. Spectra for each time interval (N = 1024 resulting in dof = 20) were averaged across the VLF band of interest with 50% overlap (band-averaging increases dof to 84, significance level = 0.125), removing effects from surface-gravity and infragravity waves. These VLF spectral averages were computed for all levels between the near-bottom and near-surface levels (z/h 0.42 to 0.84 for ADCP 6 and 0.36 to 0.84 for ADCP 4). Coherence and phase were averaged across the VLF band in a similar manner. The reference level (z/h), or first time series, for computation of coherence was 0.84 for ADCP 6 and 0.36 for ADCP 4. The reference level was near-bottom for ADCP 4, as most of the dominant energy

was contained lower in the column than at ADCP 6 (Figure 4). Additionally, using a near-bottom reference level excluded most surface noise present at the location. This process was repeated through the entire exercise period, and results were plotted on a two-dimensional plot of time versus normalized depth (time-depth stack). Thus, the average VLF energy, coherence, and phase for particular levels or times are inspected with regard to neighboring levels and time periods throughout the exercise (Figure 5).

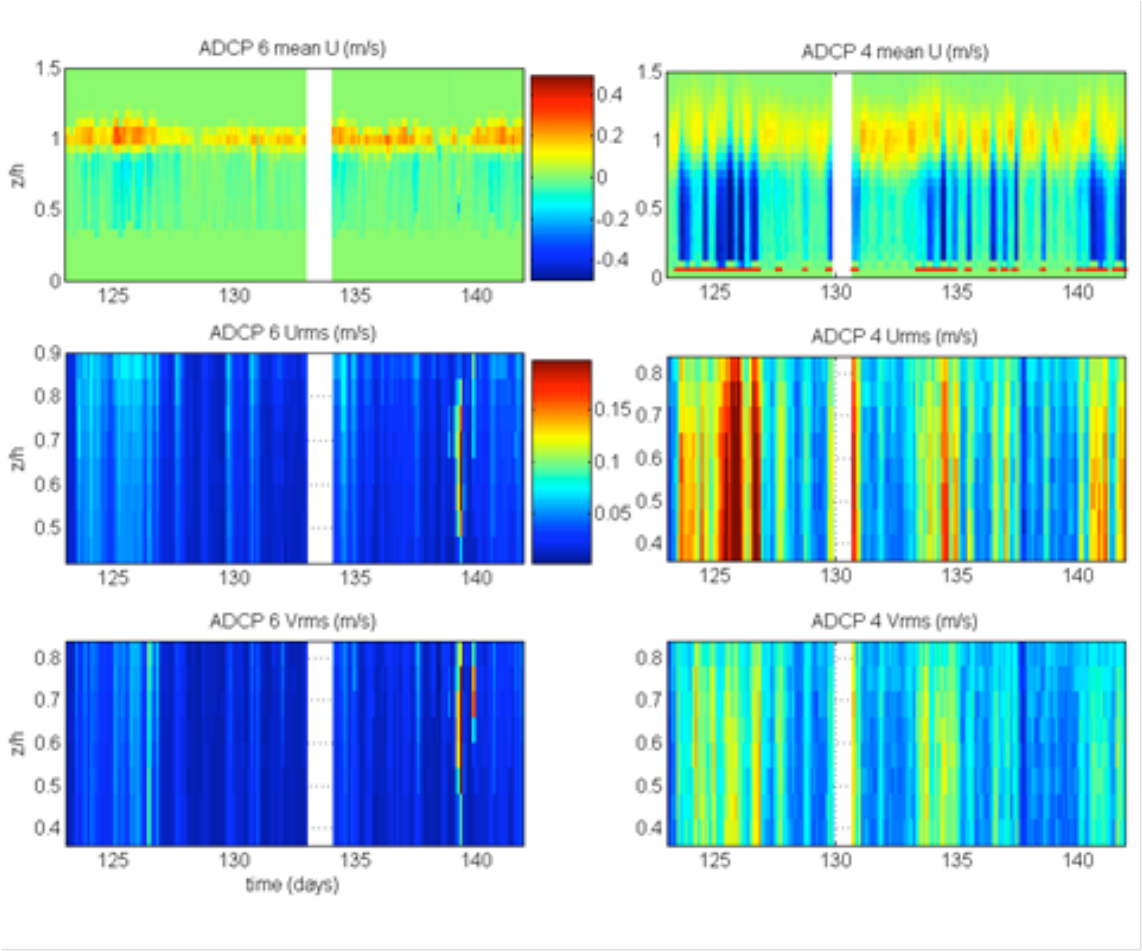

Figure 4. Hourly mean U (top), 3-hour VLF root mean square (rms) U (middle), and VLF V_{rms} (bottom) for ADCP 6 (left) and ADCP 4 (right). The red line in ADCP 4 mean U denotes when the instrument location is within the surf zone ($H_{rms}/h > 0.3$).

To better physically understand the results of the VLF energy obtained through the above processes, energy values were translated into root mean square (rms) velocities. VLF U_{rms} and V_{rms} were calculated by integrating across the VLF band of interest (Figure 4). The resulting velocities were presented in the same two-dimensional plot style.

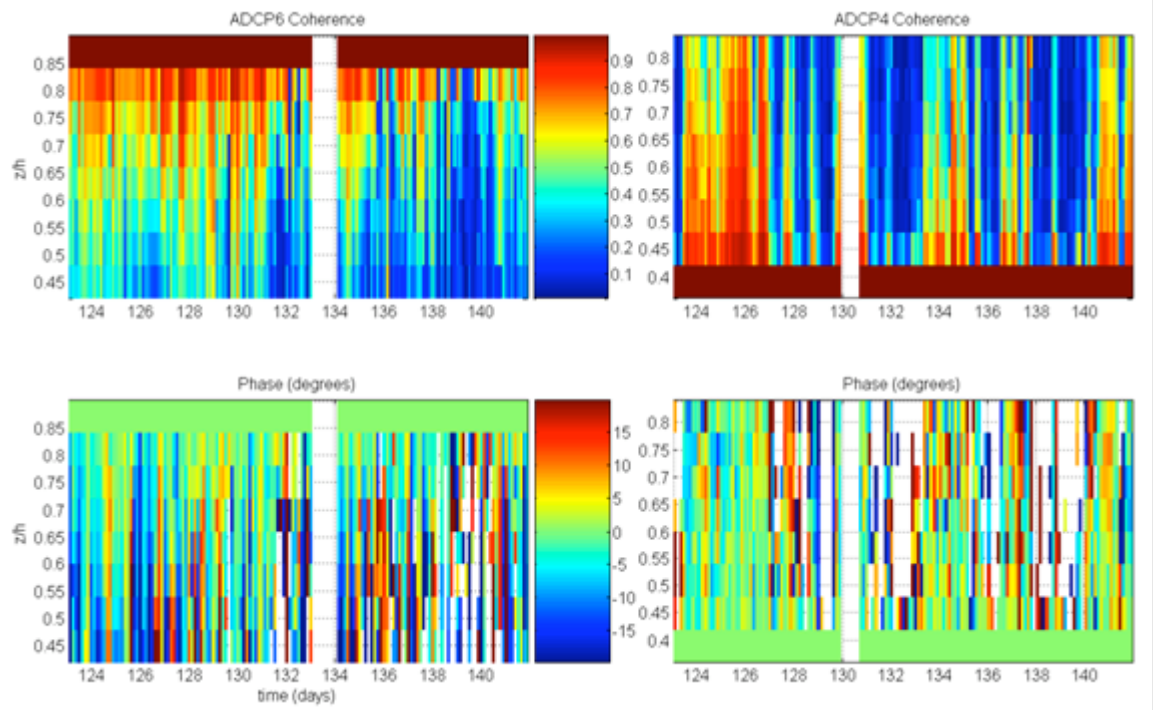

Figure 5. VLF band-averaged cross-spectral coherence and phase for ADCP 6 and ADCP 4. Values are computed between near-surface and near-bottom levels for 3-hour intervals. Reference levels (1.0 coherence) are near-surface for ADCP 6 and near-bottom for ADCP 4. Phase values are plotted for coherence values above 95% significance level.

D. CROSS-ROTARY ANALYSIS

Cross-rotary analysis (XROT) determines a two-sided inner and outer coherence amplitude and phase for a pair of two-dimensional time series (McNally et al., 1989; Mooers, 1973). This allows the author to inspect the series pairs as they rotate in different directions: positive frequencies show rotation of the reference time series rotating in the positive direction from a cardinal axis (CCW) and negative frequencies denote a series rotating in the negative

direction (CW). See Appendix A for greater detail. The inner coherence shows when the series pairs rotate in the same direction (co-rotate), and outer when the series pairs rotate in opposite directions (counter-rotate). XROT analysis was computed in a similar manner as the spectral analysis mentioned above (N = 3600 resulting in dof = 6; band-averaging increases dof to 84, significance level = 0.125), resulting in three-hour average VLF XROT values plotted in a time-depth stack. Averages for both inner (co-rotating) and outer (counter-rotating) XROT coherences were calculated over both positive (CCW) and negative (CW) VLF frequency bands of interest (Figures 6 and 7).

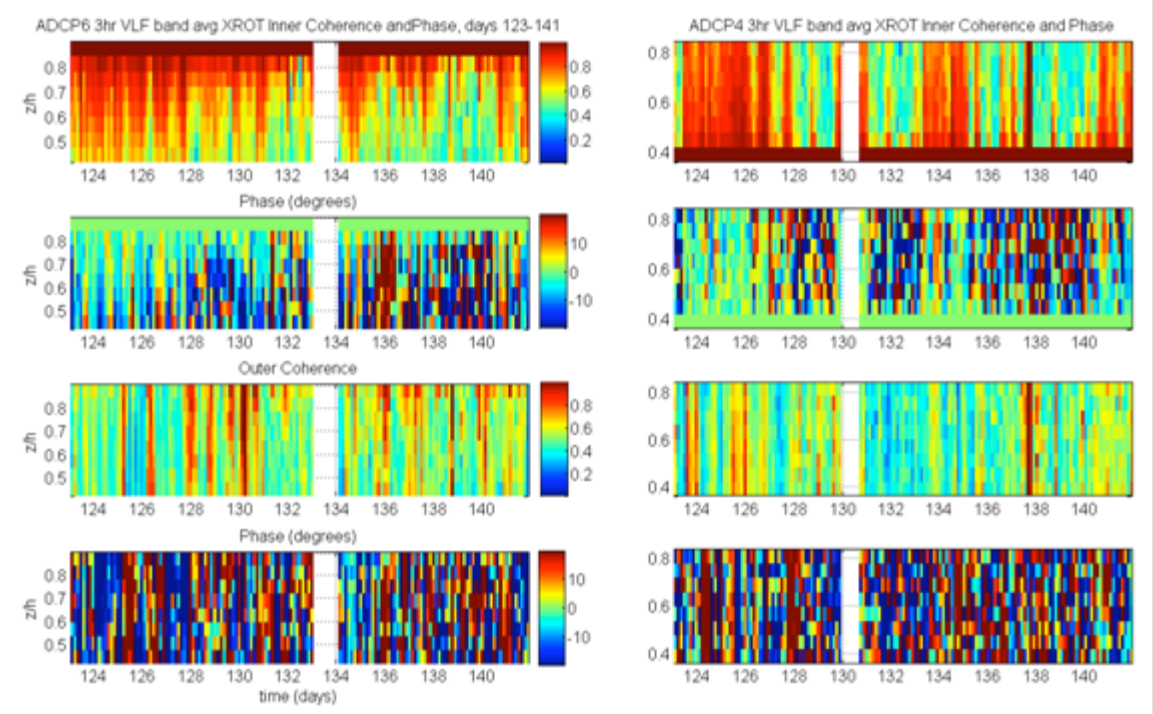

Figure 6. VLF band-averaged XROT inner (co-rotating series, top two rows) and outer (counter-rotating, bottom two rows) coherence and phase for positive (CCW) frequencies. Phase values are plotted for coherence levels above 95% significance level.

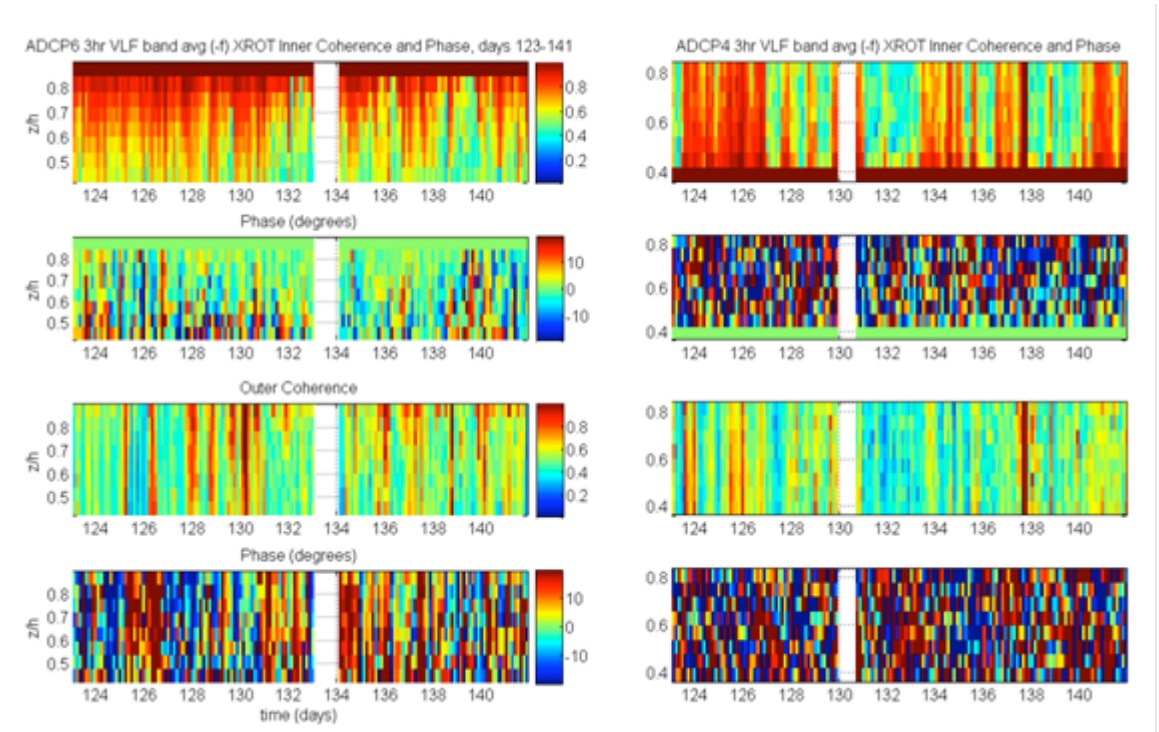

Figure 7. Same as Figure 6 for negative (CW) frequencies.

E. COMPLEX CORRELATION

Complex correlation analysis determines the average angular displacement and correlation between a pair of complex velocity vectors (Kundu, 1976). The analysis allows the author to differentiate between temporal (τ) and rotational (α) shifts between time series pairs. For more details, see Appendix B. This analysis was computed for all isolated high-energy pulse data from ADCP 6. Pulses were manually isolated to encompass the onset and termination of the primary and sustained offshore U throughout the water column and minimize inclusion of ambient velocity patterns. Pulses were randomly selected from ADCP 4 data and isolated in the same manner. For each pulse, analysis was computed for every level between the near-bottom and near-surface using aforementioned reference levels. Values of correlation, phase, and time lag were gathered for each computation and plotted against respective pulse characteristics and ambient conditions (Figure 8).

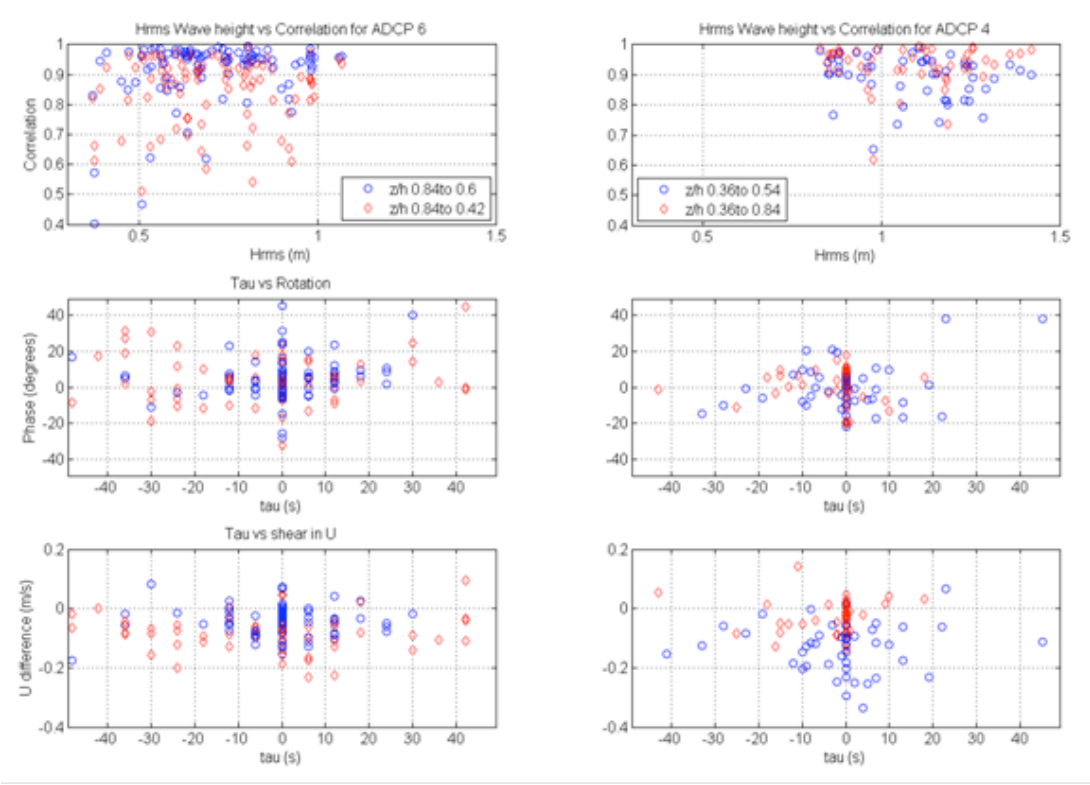

Figure 8. Bulk complex correlation values for ADCP 6 (left) and ADCP 4 (right), showing mid-column (circle) and full-column (diamond) relationships. Correlation (top row) is shown versus H_{rms} (root mean square wave height), while the phase (middle row) and shear (U difference, bottom row) of each pulse is shown versus time lead/lag (τ).

For this paper, two views of the complex correlation results within the water column are presented: full- and mid-column. Full-column results are the complex correlation values between the near-bottom normalized depth and the near-surface level at each location, i.e., illustrating the results from the full, analyzed water column. Similarly, mid-column results are the values between the reference level, either near-bottom or near-surface dependent on the location, and a normalized depth in the middle of the water column.

The offshore shear in Figure 8 was determined using the same reference levels. The difference in U is calculated by subtracting the maximum offshore U at the mid-/full-column depth from the maximum offshore U at the reference depth.

F. GROUP-AVERAGING

To inspect the general structure of high-velocity pulses, a group-averaging technique yielding a mean vertical velocity profile was used. U for each Julian Day at ADCP 6 was low-frequency filtered to the VLF band of interest (f < 0.004 Hz). At ADCP 4, a band-pass filter was used (0.0005 – 0.004 Hz) to remove effects from considerable mean velocities not present at ADCP 6. Vertical U samples were then sorted into groups defined by the near-surface velocity, ranging from -0.4 m/s offshore to 0.4 m/s onshore, at that day's near-surface level. These specific near-surface levels varied based on daily sea and weather conditions. Vertical profiles were averaged within each group for each day, to result in a mean profile for different near-surface U magnitudes (Figures 9 and 10). Thus, for higher offshore velocities associated with energetic pulses, a general vertical structure can be isolated from ambient conditions and examined.

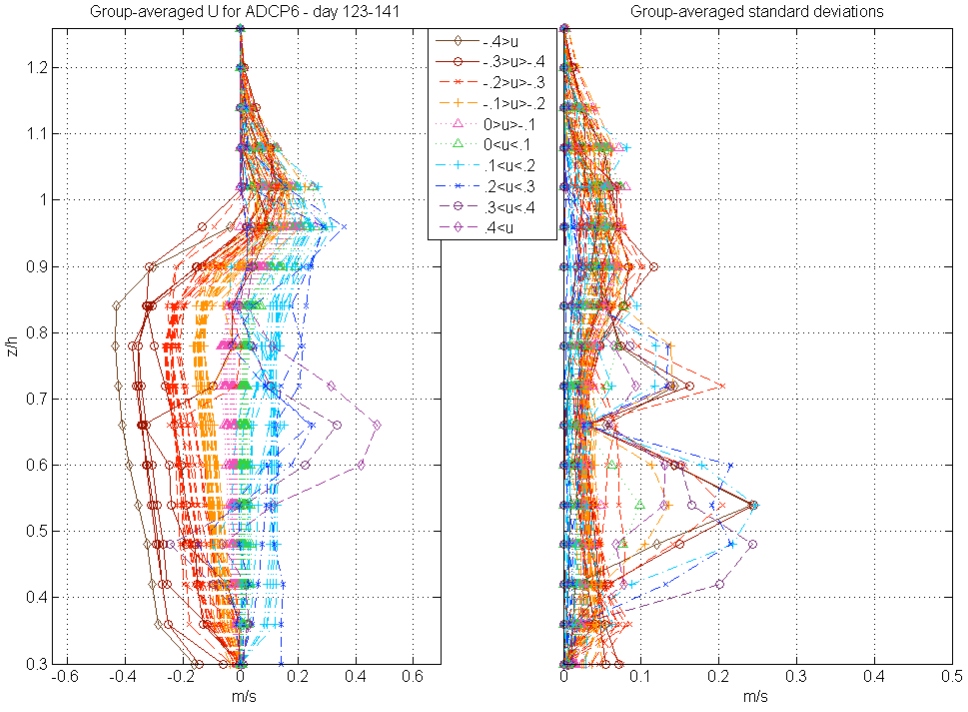

Figure 9. Group-averaged U profiles (left) and standard deviations (right) for ADCP 6. Profiles are determined from VLF U. Offshore velocities are negative.

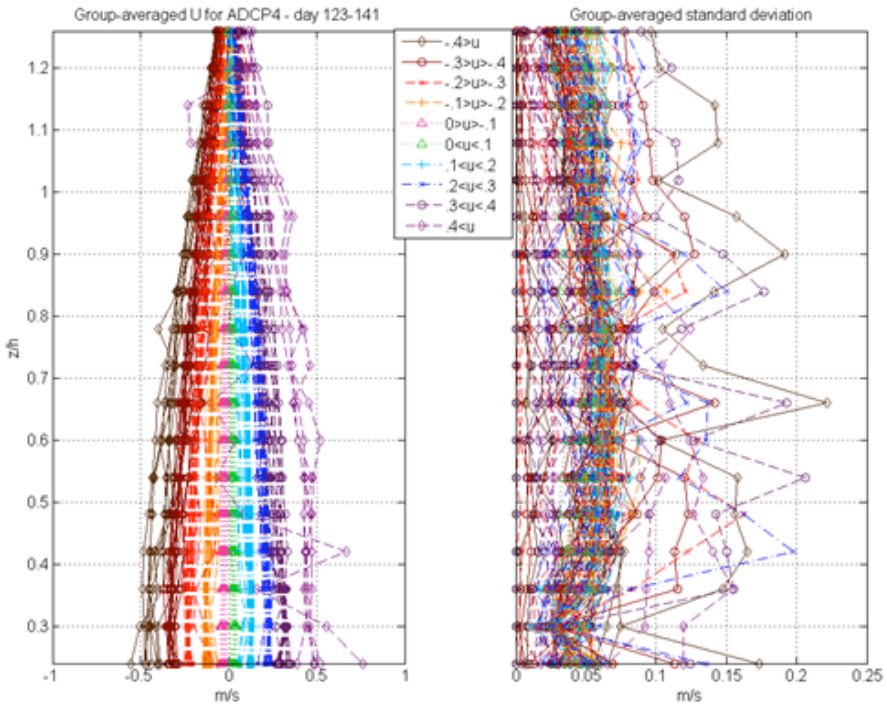

Figure 10. Same as Figure 9 for ADCP 4. Profiles are determined from bandpass-filtered (0.0005-0.004 Hz) U.

G. STOKES DRIFT CHECK

An onshore transport calculation was done for data from ADCP 4 to check the validity of the depth-relative framework. To reduce noise, vertical samples of U were averaged over time periods of one hour for the entire exercise. The positive (shoreward) U were integrated over the vertical to obtain an estimate of onshore transport (m^2/s). Theoretical values of onshore transport (Stokes drift) were also calculated for the same one-hour time periods. Onshore transport is defined as

$$Qw \approx \frac{gH_{sig}^2}{16c}\cos(\theta_w) \qquad (1)$$

where g is gravitational acceleration, H_{sig} is the significant wave height, θ_w is the shore-relative oncoming wave direction and c is the wave phase speed (Longuet-Higgins, 1953). Both the significant wave height and phase speed were one-

hour average conditions calculated from pressure sensor data. For this location, incident waves were shore normal, and θ_w was 0 degrees. The one-hour average transport estimates from the data (calculated) were compared against theoretical values for the entire exercise. Given a valid depth-relative framework for the data, the onshore estimates, calculated from the data and the theoretical value, would be equivalent.

As ADCP 4 was on the non-stationary boundary between the inner shelf and the surf zone, an index of when the instrument location was inside the surf zone was calculated. The location was defined to be inside the surf zone when

$$\frac{H_{rms}}{h} \geq 0.3 \qquad (2)$$

where H_{rms} is the one-hour root mean square wave height and h is the average water depth. Values of h and H_{rms} were calculated from the surface-corrected data within the same one-hour time periods as above. This index was indicated on the aforementioned onshore transport plot (Figure 11) and on a two-dimensional time versus normalized depth plot of one-hour average vertical profiles of U (Figure 4).

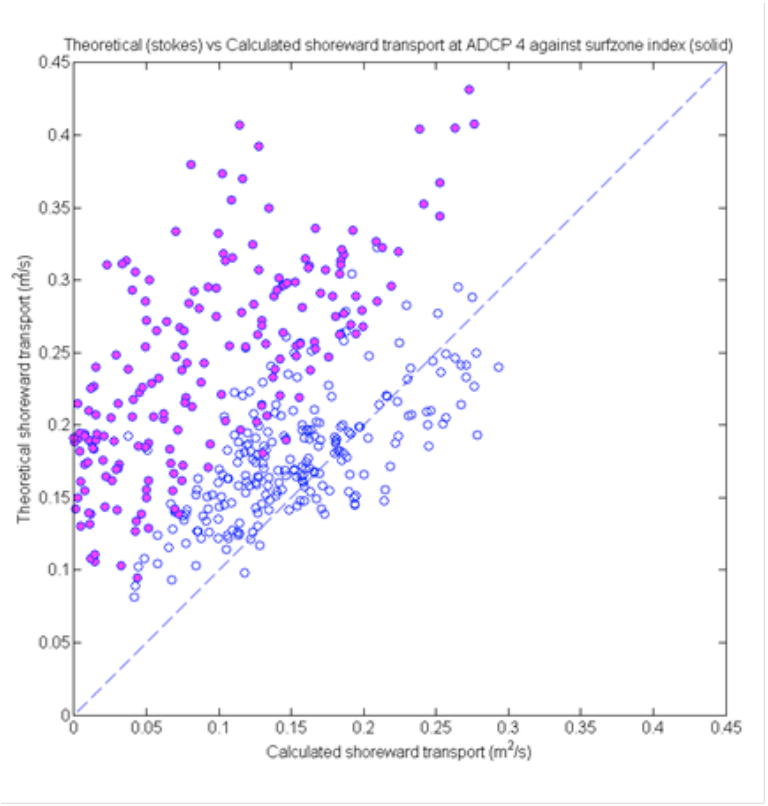

Figure 11. Scatterplot of one-hour mean values of calculated shoreward transport (from U) versus theoretical shoreward transport (Stokes drift) estimates at ADCP 4. Solid circles denote instances where wave and height conditions placed ADCP 4 in the surf zone. The blue dashed line denotes a one-to-one relationship. Regression relationship for when ADCP 4 is not in surf zone (open circles) is 0.78.

H. WAVELET ANALYSIS

Wavelet analysis' ability to show rotational and temporal relationships across time seemed ideal for analyzing aperiodic, episodic pulses in the inner-shelf. Previous visual inspection and analysis mentioned above had already shown a predominant structure in the stronger pulses (Smith and Largier, 1995; Haas and Svendsen, 2002), and the author thought wavelet analysis would provide the means to quantitatively inspect this structure further. The aperiodic nature of the pulses though, caused significant frequency spreading, such that no clear pulse signatures could be identified. Therefore, this analysis technique was unsuitable for studying these phenomena. See Appendix C for details.

THIS PAGE INTENTIONALLY LEFT BLANK

III. RESULTS

A. SPECTRA/RMS

As the rms velocity determined from the VLF spectra shows probable variability within the VLF range, large values of U_{rms} or V_{rms} depict an energetic signature within the frequency band of interest, likely due to energetic pulses. During periods when ADCP 4 is defined to be in the surf zone (Figure 4), U_{rms} and V_{rms} show greater variability and coherence is higher. These periods occur at the same time as high energy wave conditions, as seen in Figure 3. The large magnitude of Urms at ADCP 4 during these times, up to 0.5 m/s, is on the order of the highest mean U within the water column. Consequently, these pulses represent a significant portion of the observed energy within the water column. V_{rms} is lower than U_{rms} at each location, and does not constitute the primary variability associated with pulses. Coherence is higher and more consistent, above 0.6 in high energy wave conditions, throughout the water column at ADCP 4 than at ADCP 6 in the inner shelf.

Similar to ADCP 4 results, ADCP 6 shows higher coherence values and variability during the same high energy wave conditions (Figures 4 and 5). The magnitude of U_{rms} at ADCP 6 is much lower though, on the order of 0.1 m/s. As the highest mean U (~0.5 m/s) in the inner shelf are within the wave portion of the water column, the U_{rms} magnitudes in the near-surface levels are still on the order of the mean U at near-surface depths, also suggesting the pulses represent a considerable segment of the energy beneath the waves. Coherence patterns differ from ADCP 4 though, as it is contained within the near-surface levels (coherence above 0.5) in the inner shelf.

These coherence patterns suggest pulses inhabit upper portions of the water column in the inner shelf, while pulses occupy a much greater breadth of the water column in the surf zone.

Phase relationships at ADCP 4 show almost no phase offset within the water column (Figure 5). Conversely, in the inner shelf, respective phase offset values up to 20 degrees, both negative and positive, are depicted. A slight but apparent preference for a negative phase offset is observable at ADCP 6, denoting that deeper levels are offset from the near-surface level in the negative phase direction. This is compatible with observations of twisting currents over depth by Haas and Svendsen (2005) in laboratory experiments. Though the laboratory experiment represented an extreme rip event and the observations were of momentary current structures, this study's time- and frequency-averaged results compliment the previous work and highlight the presence of rotational structure to rip pulses. Phase patterns show pulses exhibit more rotation in the inner shelf, whereas they are more depth-uniform in the surf zone. As the determination of spectral phase is unable to distinguish between time and rotational offset, these relationships may be due to a lag in pulse onset at a lower normalized depth, genuine rotation, or some combination of both.

B. CROSS-ROTARY ANALYSIS

XROT analysis improves the ability to discern the types of phase relationships present over traditional spectral analysis. During high-energy conditions, when energetic pulses were prevalent, XROT analysis shows a tendency for rotational uniformity (co-rotating water column) for both CW and CCW directions. Pulses are less vertically coherent in the inner shelf and display more variability in phase.

At ADCP 4, the water column shows high inner (co-rotating) coherence for both negative and positive frequencies (Figures 6 and 7). The water column displays higher (above 0.7) and more depth-consistent coherence when the location is in the surf zone. Inspecting coherence across the experiment period, coherence patterns are switch-like, turning on high coherence during high energy wave conditions, and off during subsiding conditions. Corresponding phase values for positive frequencies (rotating in the CCW direction) are near 0

degrees, while phase for negative frequencies (CW) are more varied, ranging from -20 to 20 degrees with no directional preference. Outer (counter-rotating) coherence, on the other hand, shows a significantly decreased relationship, with no discernable phase pattern.

The drastic contrast between outer and inner relationships describes the water column as being rotationally-uniform, with the entire water column rotating in predominantly one direction vice levels rotating opposite directions from each other. This validates that the author was inspecting physical pulse phenomena, as the pulse must physically rotate in one direction, and counter-rotation within a pulse phenomena is highly unlikely.

Inner coherence relationships in the inner shelf are shallower, contained more within the upper levels of the water column than in the surf zone. Though coherence is not as consistent with depth as at ADCP 4, high coherence (above 0.7) in the upper levels is more consistent throughout the experiment. It does not display the same switch-like behavior; rather, the level of high coherence deepens and shallows according to the same conditions. Associated phase values for positive frequencies are near 0 degrees, with an apparent tendency for negative phase values (lower depths CCW from near-surface reference level). This is consistent with both previous spectral results and other studies (Haas and Svendsen, 2005). Phase values for negative frequencies are near 0 degrees, unlike in the surf zone. Observable relationships in outer coherence within the water column are drastically diminished, with no apparent pattern in phase, again showing the water column is rotationally uniform.

The abruptness of the inner coherence values at ADCP 4, compared with the smoother, more consistent coherence in the inner shelf at ADCP 6 (Figure 6 and 7) further suggest that pulses inhabit the upper to middle portions of the water column. Given the switch-like features of coherence at ADCP 4, this transition from depth-uniform phenomena in the surf zone to a near-surface structure may happen quickly upon its departure from the surf zone.

The preponderance for co-rotating phenomena in the CW direction at ADCP 4 may be explained by the horizontal structure of the rip system. Rip currents, as part of the rip cell, are not geographically stationary phenomena, but move within the channel. This may account for some of the observed variability or tendencies in the results, but a more likely cause is the movement of the rip cell system. Rip cell movement, first introduced by Peregrine (1998), is theorized to be in the form of oscillations in either the cross-shore or along-shore direction. MacMahan et al., (2004) illustrated that predominantly cross-shore oscillations of a rip cell created energy signatures in the cross-shore direction at the wave length of a rip system, but also in the along-shore direction around wavelengths of 0 m. Signatures were not clearly defined but smeared around the wavelength value in frequency space. If velocity data were sampled near one edge of a rip cell, as it favored one side of the rip channel, the signatures could smear asymmetrically. Given primarily cross-shore oscillations of the rip cell, such energy signatures could cause potential bias in one rotational signature over the other (CCW vice CW). As the pulse would move beyond the channel into the inner shelf, no longer tied to the cell system, no such directional preference would result in the inner shelf. This is consistent with observations.

A curious feature also observed at ADCP 6 is a phase reversal (Figure 6) during high energy wave conditions, periods characterized by consistent wave energy and numerous rip pulse occurrences (Figure 3). While negative phase values are favored during these times, phase values seem to switch back and forth between positive and negative offsets within the entire column at tide-dependent intervals. Periods between such positive reversals are approximately 24 hours, corresponding to the onset of flood tide. This phase reversal is also observed, though to a lesser extent, in the traditional spectral phase plots above.

C. COMPLEX CORRELATION

Correlations between normalized depths are high for all pulses and not affected by wave height (Figure 8) or mean background velocity (not shown); such high correlations verify the pulse signatures are coherent within the water column for both locations. Pulses display more vertical rotation and time lags/leads, however, in inner-shelf than in the surf zone. Time lead/lag relationships are short (up to 20 seconds) at ADCP 4, while these relationships at ADCP 6 are longer (up to 80 seconds) and more variable. Likewise, values of rotation are smaller (up to 20 degrees) at ADCP 4 than at ADCP 6 (up to 40 degrees). As plots of both time lead/lag and phase are tight at ADCP 4 and much broader at ADCP 6, pulses in the inner shelf display more variability in rotational and temporal structure. Large vertical shear, $(U_1 - U_2)$ on the order of 0.2 m/s, is observed for both locations, though shear is greater at ADCP 4. Within the water column, shear in U is more delineated at ADCP 4, showing consistent vertical structure. No progression or pattern in shear is evident at ADCP 6, further emphasizing the variability of structure in the inner shelf.

The short time lead/lags and minimal rotation in surf zone pulses stress a depth-uniform structure. Conversely, rotation in the structure at ADCP 6 illustrates a vertical twisting of the surface-dominated pulses in the inner shelf. In addition to physical rotation, larger time lead/lags further highlight a physically-forced twist in the pulse structure, likely including significant frictional effects.

In terms of originating dynamics, reconciling this vertical twist with previously mentioned surface-domination is not straightforward. Such a vertical structure may be due to the detachment of rip pulses from the surf zone, as observed by Smith and Largier (1995). As a pulse exits the surf zone, detaching from the well-mixed shallow-water environment, the encapsulated pulse flows offshore as an isolated vortex feature. An uncomplicated example shows that as the vortex feature transits into deeper water, maintaining a similar absolute depth and density from its origination (shallow and relatively light), the rotating mass

would naturally come to inhabit levels nearer the surface. As the water mass goes offshore, shear transfers momentum to the deeper levels, possibly a reason for observed lag relationships observed in the results. This illustration is overly simple, though, neglecting numerous other forces in the nearshore region; a dynamical approach that includes mass continuity of rip pulses or wave-current interaction may explain the structure as the pulse transits into the inner shelf:.

The first approach follows the concept of mass continuity. As the pulse enters the inner shelf as a rip head, it spreads out in the horizontal, a standard observation in many rip current experiments. As the detached and isolated pulse spreads, mass continuity maintains that the depth of the pulse mass must decrease and inner shelf water from below must flow up to compensate. A theorized down flow occurs below the edges of the rip head vortex in response to this localized up flow. The rip head also incurs rotation outside the surf zone, often visible to the casual observer (MacMahan et al., 2006). While the cause of rotation is not known precisely, it is likely shear. The combination of shallowing depth and rip head rotation would produce similar results as in this study.

A more exacting approach is wave-current interaction (Smith, 2006). The "refraction force" is defined as

$$\left(M^{W} \times (\nabla \times U)\right) \qquad (3)$$

where M^{W} is onshore wave-induced transport (Stokes drift) and $(\nabla \times U)$ is horizontal shear effected by the pulse relative to the surrounding water. The cross-multiple of Stokes drift with the pulse shear results in a force away from the pulse in both along-shore directions, causing the pulse to stretch in the along-shore. The stretching of the pulse in the alongshore direction, combined with the shear-induced eddy rotation would produce localized upwelling and shallowing of structure, similar to the mass continuity case above. Again, the union of rotation and shallowing structure would yield results mirroring those obtained by this study. Unfortunately, 2D horizontal data of pulse structure is rare, and thus, investigation into the application of this force is limited.

The greater variability, suggested by the spread in values of time lag/lead and shear at ADCP 6, is consistent with the concept of an isolated vortex feature being sampled by a single-point instrument. Like the rip current in the rip channel, a rip head vortex does not occupy one geographical location but meanders and drifts according to momentum and ambient currents (MacMahan et al., 2006). As the advected vortex moves over the instrument location, different parts of the vortex in different stages of formation would be sampled, giving rise to variability in structure.

D. GROUP-AVERAGING

Group-average profiles at ADCP 6 exhibit a distinct offshore vertical tilt (Figure 9). The larger velocities are in the near-surface levels and magnitudes decrease going down in the water column. Examining the separate velocity groups, larger offshore velocities reveal a steeper tilt, up to 0.3 m/s over half the water column (0.5 z/h). Near-bottom depths contain large variability (~0.05 m/s), while this value gradually decreases towards the top of the water column. As greater offshore velocities in the group-averaged profiles are associated with energetic pulses, the vertical tilt is a characteristic of the pulses in the inner shelf. The degree of this tilt shows a significant shear accompanying the pulses, consistent with complex correlation results.

At ADCP 4 however, profiles present little vertical offshore tilt in the same below-wave portion of the water column (Figure 10). Variability is nearly uniform throughout the column (~0.08 m/s) for all group magnitudes. Pulses in the surf zone do not display as accentuated a vertical structure as when in the inner shelf.

The large variability present in the profiles and standard deviations at ADCP 6 may be indicative of the persistence of structure. Near-bottom levels at ADCP 6 showed the greatest variability suggesting that while a tilting vertical structure likely depicts the behavior of most pulses, the degree of the shear may fluctuate. The nearly identical variability in the water column at ADCP 4 signifies

a more consistent and even structure in the vertical. On the surf zone border, rip pulses show a depth-uniform velocity structure while outside the surf zone the pulses become more surface-dominant in structure displaying the greatest velocity below the region directly influenced by waves. Both observations are consistent with other results from this study and previous experiments (Haas and Svendsen, 2002; Smith and Largier, 1995), as well as both dynamical explanations introduced earlier, wave-current interaction or mass continuity.

E. STOKES DRIFT

The scatter plot of onshore transport estimates displays two groupings, divided by surf zone location (Figure 11). When ADCP 4 is outside the surf zone, the calculations from the data are nearly equivalent to the theoretical estimates, validating the depth-relative framework. When the location is inside the surf zone, however, significantly lower onshore transport is observed than theory estimates. High-energy conditions, such as days 124-126, with large swells and low tide, account for periods when ADCP 4 lies within the surf zone region (Figure 3 and 4). Examination of the one-hour average vertical profiles during these times shows the water column is dominated by offshore flow (Figure 4). The average profiles show strong offshore flow below the wave trough (~0.5 m/s) and weaker offshore flow in the wave portion.

This predominant offshore flow during periods of relatively high wave energy is contrary to expected Stokes drift estimations, and is seemingly not balanced by onshore wave transport. Though this imbalance is interesting, it must be noted that it is observed only at this singular location in the region, and it is not representative of the volume exchange found elsewhere along the beach, such as over the shoal. Indeed, it is the sum transport along the shore that ultimately drives the return offshore flow feeding the rip currents. The deficit of onshore flow observed at ADCP 4 when it is in the surf zone may be accounted for by increased simultaneous onshore flow over the shoal.

IV. DISCUSSION

While the transports calculated at ADCP 4 may not be indicative of the volume exchange in the surf zone, the offshore flow at ADCP 6 in the inner shelf may suggest what volume of water is leaving, and consequently the flushing time of, the surf zone. Calculating transports in the same fashion as for ADCP 4 yields a look at net cross-shore flow (Figure 12). Oscillations in the onshore and offshore flux overlie generally mirrored long-term trends. Larger transport and variability in trends exist during high-energy wave conditions (Figure 3); variability in transport shows oscillations twice daily, demonstrating a probable link to tidal variability. Offshore transport over the experiment period exceeds onshore transport, with a mean net transport of -0.01 m^2/s.

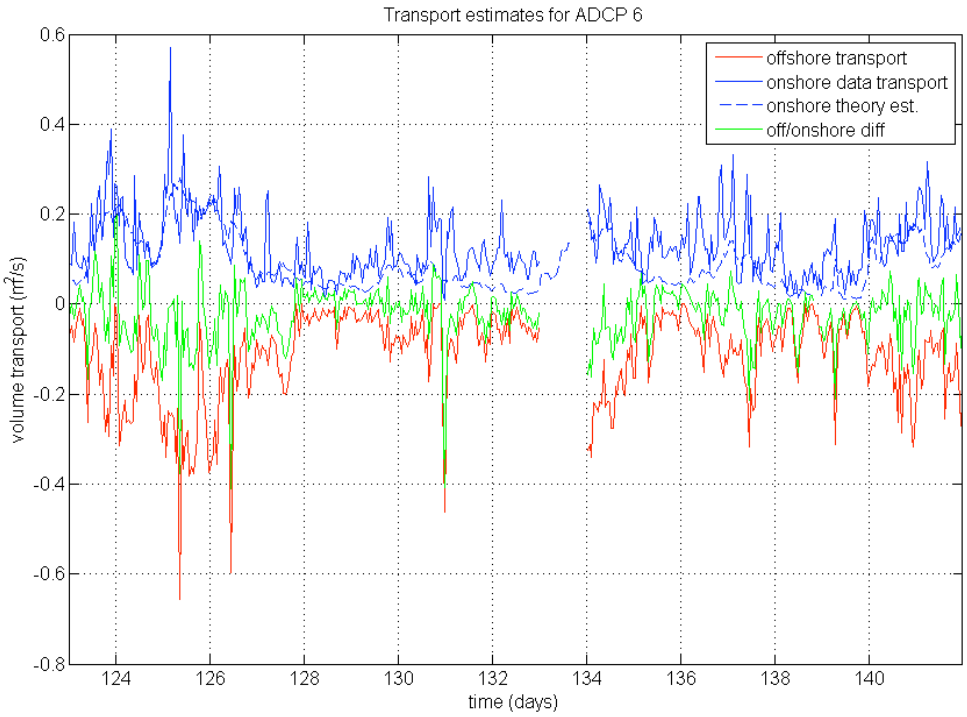

Figure 12. One-hour mean theoretical shoreward transport (Stokes drift) estimates (dashed blue line), calculated shoreward transport (solid blue line), calculated offshore transport (red line), and net transport values (green line) for RCEX. Net transport values are determined from theoretical shoreward and calculated offshore values. Offshore values are negative.

A surf zone flux can be calculated using these values and a surf zone volume. If the surf zone is assumed to be a simple inverted wedge shape with the cross-shore vertical section a right triangle, the volume of the surf zone can be calculated as approximately 1.0 $\times 10^4$ m^3. The right sides of the triangle are the 100 m surf zone width and the average breaker depth within a complete rip cell of 1.5 m; this area is multiplied by the location's average alongshore distance between two rip channels (125 m). Using a mean offshore transport of -0.1 m^2/s (Figure 12) and a 40 m rip channel width, an offshore surf zone flux of 4.0 m^3/s is obtained. This surf zone flux yields a relatively short flushing time of 40 minutes (Figure 13).

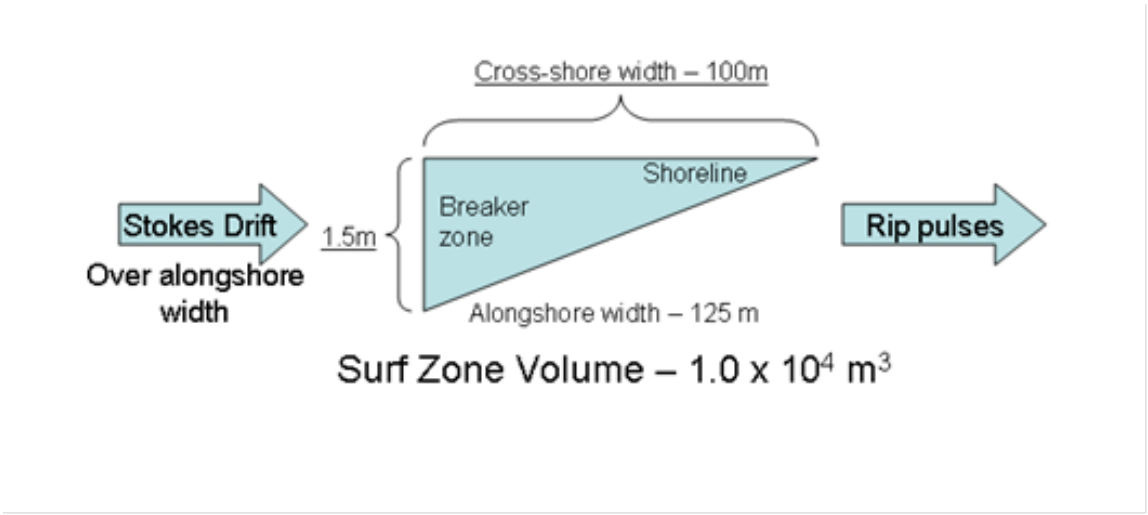

Figure 13. Conceptual drawing of surf zone inputs and outputs for purposes of calculating flushing time and volume flux. The surf zone has volume inputs from Stokes drift and outputs in rip pulses.

Current knowledge shows that rip currents meander within the channel, so assuming a static 40 m pulse width may not be accurate. The actual width of such pulses is not known, however, as there is little concrete data on the subject. Tracks from RCEX drifters exiting the surf zone into the inner shelf give a rough estimation of 30 m (MacMahan et al., 2009); this includes a great deal of variability in track direction and motion due to alongshore currents though. A review of literature shows an average width of 30-35 m (MacMahan et al., 2006),

though this is again based upon bathymetry and rip channels, not actual dimensions of rip pulses. Smith and Largier (1995) did measure the horizontal, two-dimensional structure of pulses off Scripps Pier in San Diego, CA, observing pulse widths of 15 m. They did not, however, make detailed coincident measurements of bathymetry. Using Smith and Largier's observation and known channel widths, a pulsation can be estimated to represent up to 30% of the rip channel width.

By changing the nominal width of RCEX pulses to 12 m (30% of the rip channel width), the offshore flux reduces to 1.2 m^3/s and the flushing time increases to 2.5 hours. Smaller pulse widths would assist in explaining the relative infrequency of pulse observations in the inner shelf when compared to Smith and Largier (1995). Smaller pulses, separating from the surf zone and veering away from the channel centerline, would be observed by a stationary sensor at a much lower frequency. The estimated flux also compares well with Smith and Largier's estimate and is more reasonable in terms of recognized surf zone dynamics; however, volume input to the surf zone is discounted.

To obtain a more accurate approximation of flushing time, the effect of Stokes drift must be included (Figure 13). Taking the average onshore transport (0.1 m^2/s) within the simple surf zone model, a resultant onshore flux of 12.5 m^3/s is obtained. Being much larger than the offshore estimates, there is seemingly no balance. The surf zone, by this calculation, should fill as the rip current outlets are outpaced by the oncoming transport.

This imbalance brings into question the legitimacy of familiar Stokes drift principles in the nearshore region. It is assumed that Stokes drift causes a shoreward flux into the surf zone, with volume returning offshore via rip currents or undertow. Measurements above suggest Stokes drift may overestimate this shoreward flux. If instead a strictly Eulerian frame of reference is used in the inner shelf, the apparent imbalance can be righted. Lentz, el al., (2008) found an undertow equal in magnitude and opposite of Stokes drift, resulting in zero net transport at depth. By using the difference between onshore and offshore

transport values, this undertow is accounted for. This procedure yields a net offshore transport of -0.01 m^2/s and an offshore flux of 0.12 m^3/s, effecting a 23 hour flushing time using a 12 m wide pulse. If using a larger 40 m width instead, respective values are 0.4 m^3/s and 9 hours. Of note, these estimates assume ADCP 6 sampled all existing rip pulses, which is not true. Rip currents leaving the surf zone meander and spread, rarely pulsing offshore in a straight line, such as the instrument set up. It is probable many pulses passed away from the ADCP, and hence, theses results likely underestimate the volume flux and overestimate the flushing time. Additionally, these values do not take into account the portion of water column below the lowest sampled layer, accentuating the bias.

Considering estimated e-folding time retentions of drifters within the surf zone, a proxy for surf zone flushing time, were 5.4 hours though, (MacMahan et al., 2009) the estimates accounting for smaller pulse widths and compensating offshore flow still present an accurate picture of the sampled nearshore system. Using such estimates, the pulses could export water from the surf zone, completely replacing the volume in less than a day, between 5-24 hours. Once water is exported to the inner-shelf, water may be reintroduced in shoreward currents of rip cells; the flushing does not represent a true loss of water mass to the open ocean, but a measure of the efficacy of mixing between the two regions.

V. CONCLUSIONS AND RECOMMENDATIONS

Results and previous studies reveal rip pulses exit the surf zone, detaching from the well-mixed shallow water environment, and enter the inner shelf as encapsulated vortices. These pulse eddies are shallow in structure, dominating the middle to near-surface portions of the water column, exhibiting strongest velocities just below the wave portion of the water column. A general vertical tilting structure is displayed by the pulses, as the magnitude of cross-shore velocity decreases with depth. Rotation, on the order of 20 degrees or less, is observed in such pulses in the inner-shelf. Variability in the rotational and temporal structure is high, though, as pulses show greater values of both in the inner shelf than in the surf zone. Advection of the vortex over the instrument location is a likely cause for variability. Though the dynamics forming the pulse vortex is unknown (mass continuity versus wave-current interaction), both lines of reason and aforementioned results agree that a pulse structure is present. As single-point Eulerian measurements alone cannot discern the complete structure, mainly observing the variability in the feature, amplifying work should be done to resolve physical and temporal form of such phenomena.

Consequential surf zone volume flux and flushing estimates from the results show that residence time of water in the surf zone is appreciable on the Naval operational timescale. Flushing estimate times of 5-24 hours reveal that should operationally-induced contamination of the surf zone occur, some clean-up of containment could take place before all contaminant would be flushed to the open ocean. These values are relevant to coastal communities as well. As stated by Grant, el al. (2005), flushing of the surf zone remains a major way to decrease fecal bacteria concentrations in the surf zone. Therefore, increased or decreased volume fluxes affect when the surf zone region is safe following a rise in concentration, such as increased runoff. Recirculation, via rip current cells, could reintroduce anthropogenic or biologic contaminant back into the surf zone after such flushing times, transporting contaminant alongshore.

Small naval vessels operating nearshore and swimmers should be aware of such phenomena when operating on beaches containing alongshore bars incised with rip channels. Strong offshore velocities near the surface could pose significant obstacles and hazards for vessels and swimmers. Though the individual pulses cannot be predicted, conditions favorable for the increased occurrence of strong rip pulses, such as high wave conditions combined with low tidal levels, can be identified and promulgated to naval operators. Knowledge of the structure of pulses would also be beneficial to the naval operator, as swimmers/divers could avoid the top portions of the water column when in the inner shelf. Once near the surf zone, they would encounter powerful currents regardless of location within the water column, but knowledge of the vertical and horizontal structure obtained prior to the operation could dictate correct responses to the currents or paths to lessen the obstructing flow. A collection of such conditions and morphology contributing to pulse occurrences and resulting structures is beneficial for all communities and naval units operating in the nearshore environment. Navy Meteorology and Oceanography (METOC) commands and teams could act to disseminate particular information from such a compendium to specific naval units requiring it.

Should further data collection be done, the author recommends placing the ADCP closer to the seabed and using a shorter blanking distance in order to sample more of the water column. Specifically, this placement would collect data closer to the bottom of the water column and would result in a more complete structure of observed pulses. It would also allow for more complete volume flux and flushing time estimates for the surf zone. The link between tidal forcing and observed oscillations in VLF U and V data needs to be investigated. Additionally, similar investigations of rip currents on morphologically different beaches under a variety of sea and wind conditions would be beneficial, in order to investigate whether different rip current systems display similar structure. Such steps would help create the invaluable collection of conditions and morphology contributing to pulse occurrences mentioned above.

For a more conclusive understanding of pulse configuration and nearshore dynamics, more observation of the 2D horizontal structure of rips needs to be done. With a more complete vertical profile and coincident horizontal observation, a measure of shear could be obtained to check nearshore dynamic principles, such as wave-current interaction.

THIS PAGE INTENTIONALLY LEFT BLANK

APPENDIX A. CROSS-ROTARY ANALYSIS

Cross-rotary analysis (XROT), a method of cross-spectral analysis, determines a two-sided inner and outer coherence amplitude and phase for a pair of two-dimensional time series (McNally, et al., 1989; Mooers, 1973). The inner coherence (γ_{12}) shows when the series pairs rotate in the same direction (co-rotate) and the outer (λ_{12}) when series pairs rotate in opposite directions (counter-rotate). As the coherence and phase are two-sided, they are defined over both positive and negative frequencies (ω) or directions of rotation: positive frequencies show rotation of the reference series rotating in the positive direction from a cardinal axis (CCW) and negative frequencies denote a series rotating in the negative direction (CW).

Given that two velocity vectors in complex notation are $w_1 = u_1 + iv_1$ and $w_2 = u_2 + iv_2$, inner coherence and phase is defined (McNally, et al., 1989; Mooers, 1973) as

$$\gamma_{12}(\omega) = \frac{\left|S_{w_1 w_2}\right|}{\left(S_{w_1 w_1} \cdot S_{w_2 w_2}\right)^{1/2}}, \quad -\infty < \omega < \infty \qquad (4)$$

and

$$\chi_{12}(\omega) = \tan^{-1}\left[\frac{-\mathrm{Im}(S_{w_1 w_2})}{\mathrm{Re}(S_{w_1 w_2})}\right], \quad -\infty < \omega < \infty \qquad (5)$$

$S_{w_1 w_1}$ and $S_{w_2 w_2}$ are the real inner-autospectra of the respective velocity vector series and can be written in more recognizable one-sided autospectra and cross-spectra terms of Co-spectra and Quad-spectra. Over the entire frequency range ($-\infty < \omega < \infty$), the two inner autospecta are defined (McNally, et al., 1989; Mooers, 1973) as

$$S_{w_1 w_1}(\omega) = \frac{1}{2}\left[(C_{uu} + C_{vv}) + 2Q_{uv}\right] \qquad (6)$$

and

$$S_{w_2w_2}(\omega) = \frac{1}{2}\left[(C_{\tau_x\tau_x} + C_{\tau_y\tau_y}) + 2Q_{\tau_x\tau_y} \right] \qquad (7)$$

Similarly, the complex, two-sided inner cross-spectrum $S_{w_1w_2}$ is identified as

$$S_{w_1w_2}(\omega) = \frac{1}{2}\left[(C_{u\tau_x} + C_{v\tau_y}) + (Q_{u\tau_y} + Q_{v\tau_x}) \right] + \frac{i}{2}\left[-(Q_{u\tau_x} + Q_{v\tau_y}) + (C_{u\tau_y} - C_{v\tau_x}) \right] \qquad (8)$$

In the case of the outer coherence (λ_{12}) and phase (φ_{12}), the definitions are not universally analogous. The outer cross-spectrum is defined (Mooers, 1973) as

$$Y_{w_1w_2}(\omega) = \frac{1}{2}\left[(C_{u\tau_x} - C_{v\tau_y}) + (Q_{v\tau_x} + Q_{u\tau_y}) \right] + \frac{i}{2}\left[(-Q_{u\tau_x} + Q_{v\tau_y}) + (C_{u\tau_y} + C_{v\tau_x}) \right] \qquad (9)$$

The outer coherence is then written as

$$\lambda_{12}(\omega) = \frac{\left| Y_{w_1w_2} \right|}{\left(S_{w_1w_1} \cdot S_{w_2w_2} \right)^{1/2}}, \; -\infty < \omega < \infty \qquad (10)$$

and the corresponding phase is

$$\varphi_{12}(\omega) = \tan^{-1}\left[\frac{-\mathrm{Im}(Y_{w_1w_2})}{\mathrm{Re}(Y_{w_1w_2})} \right], \; -\infty < \omega < \infty \quad (11)$$

This powerful method of cross-spectral analysis allows the author to inspect the series pairs as they rotate in different directions. The author used and modified Matlab code written by Almeida (2008), determining inner and outer coherence and phase for two vector series pairs, for computational analysis within the water column.

APPENDIX B. COMPLEX CORRELATION

Complex correlation analysis determines the average angular displacement and correlation between a pair of complex velocity vectors (Kundu, 1976). Using this analysis, the author can determine a weighted average phase angle, degree of correlation, and time lag between vector time series.

If a 2D horizontal velocity vector is expressed as $w(t) = u(t) + iv(t)$, then the complex correlation coefficient two vector series pairs is defined (Kundu, 1976) as

$$\rho = \frac{\left\langle w_1^*(t) w_2(t) \right\rangle}{\left\langle w_1^*(t) w_1(t) \right\rangle^{\frac{1}{2}} \left\langle w_2^*(t) w_2(t) \right\rangle^{\frac{1}{2}}} \qquad (12)$$

This normalized inner product indicates a degree of correlation between the velocity pairs. The average angular displacement between series pairs is determined by the corresponding phase angle α. Average displacement is defined as the counterclockwise angle of the second vector $w_2(t)$ from first vector $w_1(t)$:

$$\alpha = \tan^{-1} \frac{\left\langle u_1 v_2 - u_2 v_1 \right\rangle}{\left\langle u_1 u_2 + v_1 v_2 \right\rangle} \qquad (13)$$

This average is not an arithmetic mean but a weighted value based upon the instantaneous velocity vector magnitudes.

As the analysis from a pair of vector series yield a solution set of length t, the time (τ) of the maximum correlation allows temporal relationships to be observed. Much like an autocorrelation plot, τ shows any time lead/lag between the series pairs. If maximum correlation occurs at τ = 0, then no temporal shifts are detected. If maximum correlation occurs instead at some other value τ, series w_1 leads w_2 by τ time steps.

The author used and modified Matlab code written by Almeida (2008) and MacMahan, determining and plotting ρ and α.

THIS PAGE INTENTIONALLY LEFT BLANK

APPENDIX C. WAVELET ANALYSIS

Wavelet analysis is analogous to Fourier spectral analysis but can be used with time series containing nonstationary power at a range of frequencies. Using wavelet analysis allowed the author to use conceptually similar spectral analysis techniques to examine the pulses. Like Fourier analysis, wavelet analysis involves transforming a time series into a series of coefficients. The signal is reconstructed by adding wavelets of different scales and translations, akin to the addition of sine and cosine functions of differing periods in Fourier analysis. The wavelet analysis results in a power spectrum in time-frequency (or periodicity) space, such that dominant modes of variability can be identified through the data's time period.

This study used the methods described by Torrence and Campo (1998) and Grinsted et al. (2004) for continuous wavelet analysis and cross-wavelet analysis. Programs available from their websites and toolboxes were modified to use the ADCP data and generate wavelet spectra. Methods for the co-rotational cross-wavelet analysis, outlined by Hormazabal et al. (2004), were computed using further modified programs, in order to use both positive and negative frequencies, necessary for rotary wavelet transforms.

This study used the Morlet wavelet as the basis function used for wavelet transform. This function serves a similar purpose as a windowed Fourier transform in spectral analysis. The Morlet wavelet allows good identification and isolation of periodic signals, as it provides a balance between localization of time and frequency (Grinsted et al. 2004).

Using a Morlet wavelet, the normalized continuous wavelet transform (WT) of a time series is defined as:

$$W_n(s) = \sqrt{\frac{\partial t}{s}} \sum_{n'=1}^{N} x_{n'} \psi_o[(n' - n)\frac{\partial t}{s}] \qquad (14)$$

where x_n is a time series (n = 1,…,N) and ψ_0 is the wavelet basis function (Grinsted et al., 2004). The wavelet function is written as a function of η, a nondimensional "time" parameter. The wavelet is stretched in time by a varying scale (s) so that $\eta = s \cdot t$. In practice, it is more efficient to apply the convolution in Fourier space, yielding

$$W_n(s) = \sum_{k=0}^{N-1} \hat{x}_k \hat{\psi}^*(s\omega_k) e^{i\omega_k n \partial t} \qquad (15)$$

where $\hat{x}$ is the discrete Fourier transform of x_n, and ω_k is the positive angular frequency based on N (one-sided). Wavelet power is $|W_n(s)|^2$ (Grinsted et al., 2004; Torrence and Campo, 1998). As Liu et al. (2007) have noted though, this definition does not produce a physically consistent wavelet power spectrum and shows biases in the low frequencies. Hence, the power defined above was divided by its associated scale to rectify this bias. This power spectrum was plotted with the cone of influence (COI) and contours showing the 5% significance level. The cross-shore velocity component time series were run through WT analysis.

As the wavelets deal with finite-length time series, errors occur at the beginning and end of the resulting spectrum. Techniques used by the available programs overcome these errors by padding the time series with zeros before computing the wavelet transform. This introduces discontinuities at the endpoints with larger scales. The COI shows where these edge effects become important. Outside the COI, results contain errors and may not represent the true period or energy.

This study used 20 suboctaves per octave (the difference between two frequencies related to each other by a factor of two) and a maximum scale of 0.125 days. The highest resolved periodicity corresponded to a period of 1.4 minutes (0.00097656 days) and the lowest resolved periodicity to 3 hours (0.125 days).

The cross-wavelet transform (XWT) of two time series x_n and y_n shows where the time series share common power in time-frequency space. It is defined as $W^{XY} = W^X W^{Y*}$ where * denotes complex conjugation (Grinsted et al., 2004). The XWT spectrum was also plotted with the COI and 5% significance level contours. As the rotational aspects between the time series are of interest in this study, the relative phase was also plotted with the power spectrum. The XWT analyses were computed using both cross- and along-shore components of the time series, and between the cross-shore velocity time series.

As outlined by Hormazabal et al. (2004), the co-rotational cross-wavelet transform (XROT) is used to estimate the joint energy contained by two time series for components rotating in the same direction. For two time series with rotary wavelet transforms in the clockwise (CW, -) and counterclockwise (CCW, +) direction, the power spectrum is

$$S_n^{\pm xy}(s) = W_n^{\pm x} W_n^{\pm y*} \qquad (16)$$

The CW transform is valid for ω_k >0 and inversely, the CCW transform for ω_k <0.

The phase for co-rotating wavelets show any lag or lead relationships between co-rotating components, and is defined (Hormazabal et al., 2004) as

$$\phi_n^{\pm}(s) = \tan^{-1} \frac{\Im[\langle s^{-1} S_n^{\pm xy}(s) \rangle]}{\Re[\langle s^{-1} S_n^{\pm xy}(s) \rangle]} \qquad (17)$$

where $\Re$ and $\Im$ are the real and imaginary parts, respectively, of the smooth, co-rotating XROT power spectrum.

Hormazabal et al (2004) defines the coherence squared as

$$^{\pm}\gamma_n^2(s) = \frac{\left| \langle s^{-1} S_n^{\pm xy}(s) \rangle \right|^2}{\langle s^{-1} S_n^{\pm x}(s) \rangle \langle s^{-1} S_n^{\pm y}(s) \rangle} \qquad (18)$$

The coherence gives an indication of the correlation between rotary components that are rotating in the same direction as a function of time and periodicity. Coherences near one show a high similarity between the time series, while coherences near zero show no relationship. Phase from the XROT spectrum

was plotted only where coherence was above 0.7 to help identify correlated events in the RCEX data sets. Phase plots were computed using near-surface and near-bottom time series for all three days, as well as between near-surface velocities on days 125 and 126.

As the features of interest in this study were single pulses, some spread of power in the frequency domain was expected. Rotational and phase relationships of the pulses were the primary items of interest. As long as these aspects of the pulse could be ascertained from the analysis results, frequency spreading was not a major concern. Upon initial non-conclusive results, however, the author manufactured a time series data set containing a synthetic pulse on the order of magnitude and length of the observed pulses (0.5 m/s for 15 minutes). The time series set was analyzed in the same fashion as above in order to aid in interpreting results. To easily generate a pulse and reduce sidelobing, the pulse shape was sinusoidal. The pulse overlaid random noise of lesser magnitude (0.1 m/s). Rotation angles and time lags were varied prior to analysis. The first run was between a strictly positive cross-shore pulse (onshore-directed) and a pulse rotated 90º in the CCW direction to be positively along-shore. A time lag of 5 minutes was used. This analysis was repeated with no time lag. Next, the pulse in the second time series was rotated by 30º in the CCW direction. This configuration was analyzed with and without a 5 minute time lag.

No conclusive observable rotational or temporal relationships were present in the results. In general, it was hard to identify specific features linked to the pulses. The extensive spreading of energy in time and periodicity prevented an unambiguous correlation between power events and pulse occurrences. This was most evident in the synthetic pulse WT and XWT analyses (Figure 14); the resulting power events were not localized in period, and the author was unable to concisely link a specific relative rotation to the power event or pulse occurrence. Spreading was expected in the frequency (periodicity) domain, but not in the time domain or to the extent observable in

results. This was most likely due to the computational inference of frequency from one pulse event in a sample time period. Furthermore, any rotational and temporal relationships that may have been present in the data could not be separated or identified using wavelet techniques, as the results did not show comprehensible differences between time and rotational lags. This was most apparent in phase-shifting present in results from XROT analysis (Figure 14).

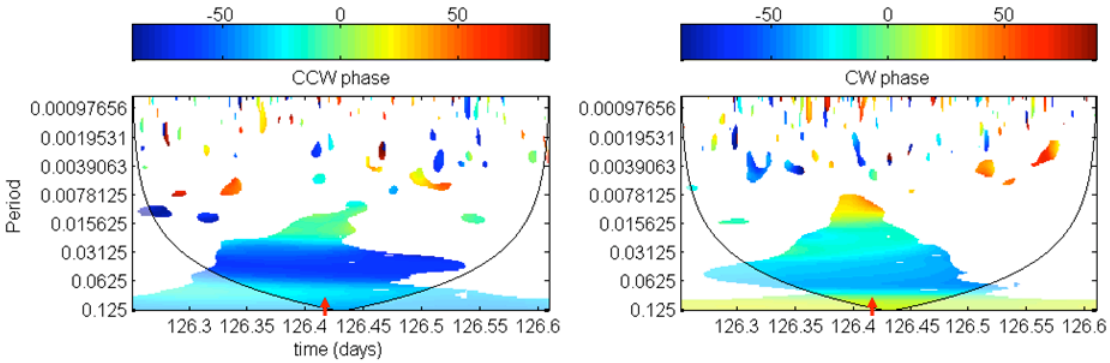

Figure 14. XROT wavelet analysis for synthetic pulse. Color indicates the phase angle (in degrees) between the corotating components of both series. Phase is only plotted where the co-rotating coherence is above 0.7. Shaded regions outside the COI show where edge effects are important. Period (in days) is plotted along the y axis while time (in Julian day) is plotted along the x axis. Red arrows indicate the time of the maximum pulse velocity.

THIS PAGE INTENTIONALLY LEFT BLANK

LIST OF REFERENCES

Almeida, F. (2008). *The Influence of Wind on HF RADAR Surface Current Forecasts*. Retrieved from Naval Postgraduate School Digital Theses.

Fewings, M., Lentz, S. J., & Fredericks, J. (2008). Observations of Cross-Shore Flow Driven by Cross-Shore Winds on the Inner Continental Shelf. *Journal of Physical Oceanography*, 38, 2358-2378.

Ganella, J. (1972). A Rotary-component Method for Analysing Meteorological and Oceanographic Vector Time Series. *Deep Sea Research*, 19, 833-846.

Grant, S. B., Kim, J. H., Jones, B. H., Jenkins, S. A., Wasyl, J., & Cudaback, C. (2005). Surf Zone Entrainment, Along-Shore Transport, and Human Health Implications of Pollution from Tidal Outlets. *Journal of Geophysical Research*, 110 (C10025). doi:10.1029/2004JC002401, 1-20.

Grinsted, A., Moore, J. C., & Jevrejeva, S. (2004). Application of the Cross Wavelet Transform and Wavelet Coherence to Geophysical Time Series. *Nonlinear Processes in Geophysics*, 11, 561-566.

Haas, K. A., & Svendsen, I. A. (2002). Laboratory Measurements of the Vertical Structure of Rip Currents. *Journal of Geophysical Research*, 107 (C5). doi:10.1029/2001JC000911, 1-19.

Haller, M. C. & Dalrymple, R. A. (2001). Rip Current Instabilities. *Journal of Fluid Mechanics*, 433, 161-192.

Hormazabal, S., Shaffer, G., & Leth, O. (2004). Coastal Transition Zone off Chile. *Journal of Geophysical Research*, 109 (C0). doi:10.1029/2003JC001956, 1-13.

Inman, D. L., Tait, R. J., & Nordstrom, C. E. (1971). Mixing in the Surf Zone. *Journal of Geophysical Research*, 76, 3493-3514.

Kundu, P. K. (1976). Ekman Veering Observed near the Ocean Bottom. *Journal of Physical Oceanography*, 6, 238-242.

Lentz, S. J., Fewings, M., Howd, P., Fredericks, J., & Hathaway, K. (2008). Observations of Undertow over the Inner Continental Shelf. *Journal of Physical Oceanography*, 38, 2341-2357.

Liu, Y., San Liang, X., & Weisberg, R. H. (2007). Rectification of the Bias in the Wavelet Power Spectrum. *Journal of Atmospheric and Oceanic Technology*, 24, 2093-2102.

Longuet-Higgins, M. S. (1953). Mass Transport in Water Waves. *Philosophical Transactions of the Royal Society of London. Series A. Mathematical and Physical Sciences*, 245(903), 535-581.

MacMahan, J., Reniers, A. J. H. M., Thornton, E. B., & Stanton, T. P. (2005). Surf Zone Eddies Coupled with Rip Current Morphology. *Journal of Geophysical Research*, 109 (C0). doi:10.1029/2003JC002083, 1-15.

MacMahan, J., Thornton, E. B., Stanton, T. P., & Reniers, A. J. H. M. (2005). RIPEX: Observations of a Rip Current System. *Marine Geology*, 218, 113-134.

MacMahan, J., Thornton, E. B., & Reniers, A. J. H. M. (2006). Rip Current Review. *Coastal Engineering*, 53, 191-208.

MacMahan, J., Brown, J., Brown, J., Morrison, J., Thornton, E. B., Reniers, A. J. H. M., Stanton, T., Henriquez, M., & Gallagher, E. (2009). Mean Lagrangian Flow Behavior on Open Coast Rip Channel Beaches. *Marine Geology*, submitted for publication.

McNally, G. J., Luther, D. S., & White, W. B. (1989). Subinertial Frequency Response of Wind-Driven Currents in the Mixed Layer Measured by Drifting Buoys in the Midlatitude North Pacific. *Journal of Physical Oceanography*, 19, 290-300.

Mooers, C. N. (1973). A Technique for the Cross Spectrum Analysis of Paris of Complex-Valued Time Series, with Emphasis on Properties of Polarized Components and Rotational Invariants. *Deep-Sea Research*, 20, 1129-1141.

Peregrine, D. H. (1998). Surf Zone Currents. *Theoretical and Computational Fluid Dynamics*, 10, 295-309.

RD Instruments. (1989). *Acoustic Doppler Current Profiler Principles of Operation. A Practical Primer*. San Diego, California.

Rohr, J., Hyman, M., Fallon, S., &Latz, M. J. (2002). Bioluminescence Flow Visualization in the Ocean: an Initial Strategy Based on Laboratory Experiments. *Deep-Sea Research*, 49, 2009-2033.

Shepard, F. P., Emery, K. O., & La Fond, E. C. (1941). Rip Currents: A Process of Geological Importance. *EOS Transactions, American Geophysical Union*, 31(4), 555-565.

Smith, J. A., & Largier, J. L. (1995). Observations of Nearshore Circulation: Rip Currents. *Journal of Geophysical Research*, 100, 10967-10975.

Smith, J. A. (2006). Wave-Current Interactions in Finite-Depth. *Journal of Physical Oceanography*, 36, 1403-1419.

Smith, J. A. (2008). Vorticity and Divergence of Surface Velocities Near Shore. *Journal and Physical Oceanography*, 38, 1450-1468.

Stokes, M D., Deane, G. B., Latz, M. J., & Rohr, J. (2004). Bioluminescence Imaging of Wave-Induced Turbulence. *Journal of Geophysical Research*, 109 (C01004). doi:10.1020/2003JC001871, 1-8.

Tilburg, C. E. (2003). Across-Shelf Transport on a Continental Shelf: Do Across-Shelf Winds Matter? *Journal of Physical Oceanography*, 33, 2675-2688.

Torrence, C., & Compo, G. P. (1998). A Practical Guide to Wavelet Analysis. *Bulletin of the American Meteorological Society*, 79, 61-78.

INITIAL DISTRIBUTION LIST

1. Defense Technical Information Center
   Ft. Belvoir, Virginia

2. Dudley Knox Library
   Naval Postgraduate School
   Monterey, California

3. Professor Jamie MacMahan
   Naval Postgraduate School
   Monterey, California

4. Professor Edward Thornton
   Naval Postgraduate School
   Monterey, California

5. Professor Jeffrey D. Paduan
   Naval Postgraduate School
   Monterey, California